Co-Ni-arsenide mineralisation in the Bou Azzer district (Anti-Atlas, Morocco): genetic model and tectonic implications

Tourneur Enora, Alain Chauvet, Kouzmanov Kalin, Johann Tuduri, Paquez Camille, Sizaret Stanislas, Karfal Abdelhak, Moundi Younes, El Hassani Abdelfattah

Journal Pre-proofs

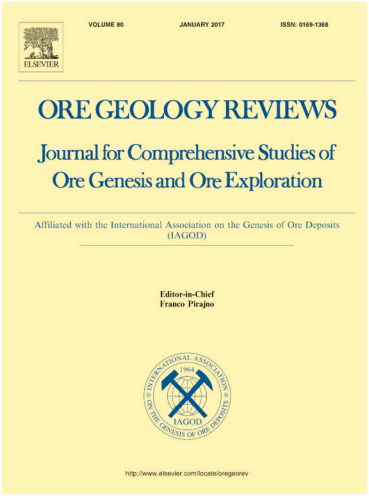

Co-Ni-arsenide mineralisation in the Bou Azzer district (Anti-Atlas, Morocco): genetic model and tectonic implications

Tourneur Enora, Chauvet Alain, Kouzmanov Kalin, Tuduri Johann, Paquez Camille, Sizaret Stanislas, Karfal Abdelhak, Moundi Younes, El Hassani Abdelfattah

PII: S0169-1368(21)00153-0
DOI: https://doi.org/10.1016/j.oregeorev.2021.104128
Reference: OREGEO 104128

To appear in: *Ore Geology Reviews*

Received Date: 23 July 2020
Revised Date: 24 December 2020
Accepted Date: 14 March 2021

Please cite this article as: T. Enora, C. Alain, K. Kalin, T. Johann, P. Camille, S. Stanislas, K. Abdelhak, M. Younes, E. Hassani Abdelfattah, Co-Ni-arsenide mineralisation in the Bou Azzer district (Anti-Atlas, Morocco): genetic model and tectonic implications, *Ore Geology Reviews* (2021), doi: https://doi.org/10.1016/j.oregeorev.2021.104128

Co-Ni-arsenide mineralisation in the Bou Azzer district (Anti-Atlas, Morocco): genetic model and tectonic implications

Tourneur Enora[1]; Chauvet Alain[1]; Kouzmanov Kalin[2]; Tuduri Johann[3,4]; Paquez Camille[5,6], Sizaret Stanislas[4]; Karfal Abdelhak[7]; Moundi Younes[7]; El Hassani Abdelfattah[7]

[1]: UMR 5243, Géosciences Montpellier, University of Montpellier, University of Antilles, CNRS, Montpellier, France

[2]: Department of Earth sciences, University of Geneva, 1205 Geneva, Switzerland

[3]: BRGM, F-45060 Orléans, France

[4]: ISTO, UMR7327, University of Orléans, CNRS, BRGM, F-45071 Orléans, France

[5]: Géosciences Réunion (LSTUR), University of La Réunion, 15, Avenue René Cassin, CS 92003, 97744 Saint Denis Cedex 9

[6]: Institut de physique du globe de Paris, University of Paris, CNRS, F-75005 Paris, France

[7]: Managem Group and CTT, Twin Centre-Tour A, BP16016, Casablanca, Morocco

Abstract

The two main types of mineralisation in the Co-Ni-As Bou Azzer district, i.e., "contact" mineralisation" and "cross-cutting" structures have been re-defined based on new field, structural, textural and mineralogical observations. The main orebodies consists of elongated lenses of massive Ni-Co-Fe arsenide minerals. These lenses occur in a core of carbonate or siliceous gangue and are almost exclusively located along the contact between serpentinite and a quartz diorite intrusion. Vein systems, cross-cutting the different lithologies, are ore-bearing only along segments in contact with the serpentinite and/or the massive mineralisation. The two orebody types share a rather similar mineralisation history, starting with a Ni-rich arsenide stage (mainly expressed within the massive mineralisation), followed by a massive Co-arsenide stage recognised in both mineralisation styles, and ending with Fe-rich arsenide and base metal sulphide stage.

Detailed field observations, microstructural, tectonic, textural and mineralogical analyses led us to propose a genetic model for the Bou Azzer ore district in which massive mineralisation was formed by alteration and transformation of previously formed breccia levels composed of serpentinite (transformed to gangue) and magnetite/spinel (transformed to Co-Ni arsenide minerals) fragments. Inversely, a tectono-hydrothermal event controlled by a NE oriented transtension generated the vein system, associated certainly with partial leaching and reconcentration of metals from the massive mineralisation because veins are principally mineralised when crossing massive orebodies. We discuss a possible temporal continuum between the two mineralisation styles: massive mineralisation,

coeval with serpentinisation (serpentine neoformation), is related to the transformation of brecciated lenses and vein mineralisation is formed as an infill of large fractures during transtensive tectonics. This model has significant tectonic implications, because serpentinite breccia lenses, favourable high-permeability environment for the massive mineralisation formation, can be compared to ophicalcic rocks developed in a context of mantle exhumation by detachment. Two types of textures can be differentiated within the massive mineralisation: i) Brecciated Massive Mineralisation, developed in the core of ophicalcic levels, and ii) Laminated Massive Mineralisation, supposed to form within ancient mylonitic serpentinite levels corresponding to intensive deformation zones. Although the geodynamic significance will not be addressed in this article, we propose and discuss an alternative model in which the presence of exhumed mantle rocks allows the formation of specific massive arsenide deposits.

Keywords: Co-Ni-As (-Au-Ag) Bou Azzer district; Hydrothermalism; Serpentinite; Vein; Massive arsenide ores; Tectonic implications

1. Introduction

Economic concentrations of Co are almost always considered as by- or co-product of mining where Co is associated with Cu and/or Ni. The only exception is the Bou Azzer Co-Ni-As (-Au-Ag) district in Morocco that hosts the only mine in the world where Co is produced as a primary product. No satisfying genetic model has been proposed so far in the abundant literature regarding the Bou Azzer district. Five main Co deposit types are presently identified worldwide and associated to different geological settings: 1) sediment-hosted stratiform Cu-Co deposits such as the Central African Copper Belt in DRC and Zambia in which Cu and Co are mostly concentrated by diagenetic processes (Cailteux et al., 2005; Hitzman et al., 2012); 2) magmatic sulphide deposits such as the giant Noril'sk-Talnakh, Sudbury and Kambalda Ni-Cu (-PGE-Co) deposits in Russia, Canada and Australia, respectively (Arndt et al., 2005; Naldrett, 2005); 3) secondary concentrations within lateritic profiles, such as the Koniambo Ni (-Co) deposit, in New Caledonia (Freyssinet et al., 2005; Butt and Cluzel, 2013); 4) Mn-nodules and Co-rich crusts on the oceanic seafloor (Manheim and Lane-Bostwick, 1988; Hein and Koschinsky, 2014); and 5) the five-element hydrothermal vein type (Bi-Co-Ni-Ag-As±U), whose formation is related to the involvement of methane as reducing agent with the circulation of connate brines, in crustal thinning environments in continental rifting and crustal thinning environments (Bastin, 1939; Kissin, 1992; Markl et al., 2016; Burisch et al., 2017). Recent works also tentatively suggest (Dolansky, 2007; Burisch et al., 2017), mainly based on similarities in the mineral assemblage and fluid signatures that the Bou Azzer district may belong to the five-element veins deposit type.

The Bou Azzer mining district hosts an enigmatic type of Co-Ni-As (-Au-Ag) mineralisation located at the vicinity of hydrated ultramafic rock complex (serpentinite) (Leblanc, 1975; Saquaque et

al., 1989; Ennaciri, 1995; Hefferan et al., 2000, Kreissl et al., 2018; Ikenne et al., 2020). Although the paragenesis is rather well-known (Leblanc and Billaud, 1982; Ennaciri, 1995; Ennaciri et al., 1995; Ahmed et al., 2009; Gervilla et al., 2012), the mode of formation and the structural constraints on the mineralisation remain unsolved so far. Indeed, although recent models are based on hot brines circulation within the basement rocks during a major extensional tectonic episode at the end of the Variscan orogeny (e.g. Essarraj et al., 2005, Oberthür et al., 2009), some other assumptions argue for a five-element veins deposit type (Burisch et al., 2017), suggest the deposits may have been initiated at high-temperature (>500°C, Gervilla et al., 2012) or may be also polyphase during the Neoproterozoic orogeny (Leblanc, 1975; Ennaciri et al., 1997; Tourneur et al., 2019).

Most of the authors agree that serpentinite rocks are the source for Co and Ni, leached and concentrated by hydrothermal fluid circulation, because the main ore bodies are hosted at the vicinity of a serpentinite complex (e.g. Leblanc, 1975; Ennaciri, 1995). However, the significance of the geodynamic context in terms of prerequisite for ore formation in this particular environment has never been addressed so far and structural constraints remain strongly lacking in all studies devoted to the Bou Azzer district. Recently, serpentinite occurrences worldwide have been described in tectonic environments where ultramafic mantle rocks are exhumed either in intra-continental extensional setting (Lagabrielle and Bodinier, 2008), or in hyper-extended rift margins at the ocean–continent transition (OCT; Boillot et al., 1987; Manatschal, 2004, Manatschal et al., 2006), among others. Mostly, serpentinisation occurs because of seawater circulation through the underlying mantle, and this process shares some common features with the formation of seafloor and sub-seafloor massive sulphide deposits (Richardson, 1987; Alt, 1995; Alt et al., 1996). In this last example, percolating seawater interacts with the oceanic crust mainly composed by gabbro and basalt in order to form massive sulphide mineral accumulations enriched in Cu, Zn, Pb, Au, and Ag. However, it has been recently demonstrated that, in the setting of mid-ocean ridges, ultramafic rocks may also exhumed along slow spreading ridges and host black smokers-like hydrothermalism yielding Cu-Fe-Ni-Co-Zn-rich ore occurrences (Coltat et al., 2019). No example of a similar process involving leaching and hydrothermal alteration of the mantle has been discussed and proposed so far for the Bou Azzer Co-Ni-As (-Au-Ag) district.

This paper integrates the results of a field study and structural, textural, mineralogical, and geochemical analyses of the Co-Ni-As (-Au-Ag) mineralisation at Bou Azzer. A model of formation is proposed and discussed taking into account the various mineralisation types, their distribution and specific geometry, as well as their mineralogical characteristics. It is also discussed if both mineralisation styles (massive lenses and veins) could have formed during continuous mineralisation events. The continuity is suggested by similar paragenetic sequence beginning with a Co-arsenide stage in both mineralisation types. However, the structural context of formation differs from emplacement in permeable and brecciated zones between serpentinite, quartz diorite and Upper Neoproterozoic volcanic rocks for the massive bodies, and ore formation in large fractures for the vein

mineralisation. The role and the significance of several parameters such as pre-existing serpentinite breccias along extensional fault/detachment, in-situ transformation processes allowing the formation of Co-Ni minerals at the expense of spinel/magnetite or significance of serpentinite as a major contributor to the leaching, transport and capture of the metallic phases have been highlighted. Finally, a tentative of integration of the Bou Azzer district in a new model of formation of "Massive Arsenides" alternative that involved hydrothermal fluid circulation in an ultramafic rock complex is proposed and discussed. Such a revisited ore-forming model constitutes a key for future exploration targeting for Co-Ni deposits essentially due to the new definition of orebody characteristics and geometry.

2. Geological setting

2.1. The Moroccan Anti-Atlas

The Moroccan Anti-Atlas is located in the southern part of Morocco and belongs to the northern edge of the West African Craton (WAC) and bordered to the north by the South-Atlasic Fault (Fig. 1). It comprises a succession of inliers that are broadly oriented WSW/ENE and characterised by Proterozoic cores overlain by Palaeozoic (mostly Cambrian) sedimentary rocks (Choubert, 1963). The Major Anti-Atlas fault (MAAF) separates two domains: the eastern domain including the Jbel Saghro, Siroua and Ougnat inliers, whereas the western domain includes nearly 10 inliers. The Bou Azzer-El Graara thus occupies a central position in the Anti-Atlas and is located exactly along the MAAF (Fig. 1). Field relationships also suggest that the Eastern Anti-Atlas only exposes Neoproterozoic terranes, while the Western Anti-Atlas exposes a Palaeoproterozoic basement overlain or intruded by Neoproterozoic sedimentary, volcanoclastic and granitoid rocks (Hollard et al., 1985). Four orogenic cycles affected the Anti-Atlas area during the Palaeoproterozoic (Eburnean: Barbey et al., 2004; Thomas et al., 2004; Ennih and Liégeois, 2001), the Neoproterozoic (Panafrican: Gasquet et al., 2005; Tuduri et al., 2018a), Palaeozoic (Variscan: Burkhard et al., 2006) and the Caenozoic (Alpine: Missenard et al., 2006). The Proterozoic events, mostly concerned by this study, are the most significant and according to Choubert (1945) and Choubert and Faure-Muret (1980), they have been historically divided into three main lithostratigraphic units called Precambrian I (PI), Precambrian II (PII) and Precambrian III (PIII) then grouped in Supergroups, Groups, Subgroups, Formations, Members and Suites with local names and geographical justifications (Thomas et al., 2004), fact that not really simplified the geological understanding in our opinion. Indeed, we have chosen here to present the lithology with the ancient nomenclature followed by a recent proposition of simplification by Tuduri et al. (2018a).

Although PI terranes were previously attributed to the Palaeoproterozoic, some have been reinterpreted as Neoproterozoic in age, like PII and PIII. PI is essentially made of Palaeproterozoic

crystalline rocks and is only observed in the Western Anti-Atlas (Ennih and Liegeois, 2001). The PII units are composed of grauwackes, quartzites and metasediments in which PII-related granitoids emplaced. The ophiolitic complexes of Bou Azzer and Siroua are also attributed to PII formations (Leblanc, 1975; Choubert and Faure-Muret, 1980). PIII formations consist of late volcanic units that overly PI and PII. They are represented by the Ouarzazate supergroup mainly composed of ignimbrites (Thomas et al., 2004; Blein et al., 2014). A new subdivision into two complexes (lower and upper) has been recently proposed by Tuduri (2005) and Tuduri et al. (2018a) and appears more appropriate for linking the sedimentary, volcanic and plutonic rocks to the two tectono-magmatic events that affected the Anti-Atlas. The term "complex" is herein employed because the two Neoproterozoic events that affected the Anti-Atlas cannot be described as classical orogenic events but more likely as an association between volcanism, magmatism and tectonics that strongly influences the nature of the lithologies. The particularity of these events, with strong influence of magmatism, low- to medium-grade metamorphism and deformation, justifies the distinction from classic orogenic phases. Indeed, the main tectono-magmatic events that characterise the Neoproterozoic deformation are: i) a first magmatic-tectonic event (in the lower complex) mainly associated with massive high-K calc-alkaline magmatism taking place in the core of weakly deformed meta-sedimentary complexes controlled by a transpressive tectonics (e.g., Choubert, 1963; Thomas et al., 2004; Gasquet et al., 2005; Tuduri, 2005; Walsh et al., 2012; Tuduri et al., 2018a,b); ii) a transtensive deformation (in the upper complex) associated with periods of intense silicic volcanism (multiple ash-flow caldera-forming eruptions), magmatism and volcano-sedimentary formations (Gasquet et al., 2005; Walsh et al., 2012; Tuduri et al., 2018a). Such ignimbritic sequences unconformably overlay the deformed lower complex. Indeed, these complexes are separated by a major unconformity that is associated with changes in the tectonic setting - between the compressional character of the lower complex (transpressional tectonics) and the extensional character of the upper one (transtensional tectonics)(Tuduri et al., 2018a).

In both the Siroua and Bou Azzer inliers, an uncertainty remains about the early occurrence of obduction and oceanic basin closure (suture zone) due to the supposed existence of one or two subduction zones. Several geodynamic interpretations have been proposed and discussed on this crucial point of the Neoproterozoic Anti-Atlas evolution (Gasquet et al., 2005; Bousquet et al., 2008; El Hadi et al., 2010; Walsh et al., 2012; Triantafyllou et al., 2018) but consensus has never been reached (see below).

2.2. The Bou Azzer inlier

Located in the central part of the Moroccan Anti-Atlas (Fig. 1), the Bou Azzer-El Graara inlier represents one the most famous inliers in Morocco, because first description of a Proterozoic

oceanic lithosphere was made there (Leblanc, 1975) and also because of its spectacular Co-Ni-As mineralisation. The Bou Azzer inlier has been defined as an ophiolitic complex supposed to be a Neoproterozoic suture zone (Leblanc, 1975, 1976, 1981; Bodinier et al., 1984; Gahlan et al., 2006). The inlier is parallel to the MAAF (Fig. 1b), and some faults with similar orientation were assigned to this major Anti-Atlas fault. The inlier is characterised by large amounts of serpentinised ultramafic rocks, originally mantle harzburgites and dunites, associated with gabbro and basaltic pillow lavas (Leblanc, 1975, 1976, 1981; Bodinier et al., 1984; Gahlan et al., 2006). The ultramafic units are surrounded by: i) a Cryogenian volcanic arc complex that was emplaced at *ca*. 770-760 Ma, and ii) Ediacaran volcanic and volcanoclastic rocks including the Ouarzazate supergroup and then infracambrian sedimentary sequences (Thomas et al., 2004; Walsh et al., 2012 ; Blein et al., 2014). There, the structural pattern is assumed to follow the closure of an ocean that may have driven to the obduction of the ophiolitic unit during a period bracketed between 640 and 770 Ma (Clauer, 1976; Leblanc, 1981; Thomas et al., 2004; Samson et al., 2004; Blein et al., 2014). Following the formation of the ophiolitic unit, the lower complex sequences consisting of deformed metavolcanic and metasedimentary rocks, that represent a late orogenic detrital sequence, were emplaced (the Bou Lbarod and Tiddiline groups). The latter are intruded by high-K calc-alkaline plutons of granodiorite, quartz diorite and gabbro at *ca*. 650- 630 Ma (Thomas et al., 2004; Inglis et al., 2005; El Hadi et al., 2010). The upper complex is characterised by numerous volcanic sheets, mostly ignimbritic, belonging to the Ouarzazate supergroup and deposited during a long-lived extensional-transtensional stage that began around 585-580 Ma and built up until 550-540 Ma (Mifdal and Peucat, 1985; Thomas et al., 2004; Blein et al., 2014; Tuduri et al., 2018a). Most of these rocks are composed of dacitic to rhyolitic ignimbrites and andesitic tuffs and overly all the Precambrian units of the Bou Azzer inlier. Calc-alkaline to high–K plutonic rocks continued to intrude these volcanoclastic units (Thomas et al., 2004). Both the lower and upper complex units were affected by greenschist facies metamorphism (Bodinier et al., 1984; Wafik et al., 2001). A sedimentary cover sequence composed of conglomerates and carbonate rocks overlies all the units and marks the transition to the Precambrian/Cambrian (Pouit, 1966; Bouchta et al., 1977; Tucker, 1986; Latham and Riding, 1990; Gasquet et al., 2005). This unit has been locally named the Adoudounian formation or, more recently, the Taroudant group.

2.3. The Bou Azzer Co-Ni-As (-Au-Ag-Cu) district

Three major mining districts can be defined within the Bou Azzer inlier (Fig. 1C). The Bou Azzer Co-Ni-As (-Au-Ag) district occurs in the NW and central parts and includes several dispersed ore deposits all related to serpentinite massifs (e.g. *Taghouni*, *Bou Azzer East*, *Aghbar*, *Tamdrost*, *Ambed*, *Aït Ahmane* and the Ag-rich *Tizi* one, Fig. 2). The Bleida Au (-Pt-Pd) district is located in the

south-eastern part. The third district is defined by the appearance of several small Cu-rich occurrences in the infracambrian sedimentary cover (El Ghorfi et al., 2006; Bourque et al., 2014; Maacha et al., 2015). The entire Co-Ni-As (-Au-Ag) Bou Azzer district is operated by the Compagnie de Tifnout Tiranimine (CTT), a subsidiary of Managem, a Moroccan industrial mining group.

Three main ore deposit types have been described in the Co-Ni-As (-Au-Ag) Bou Azzer district (Leblanc and Lbouabi, 1988; Ennaciri, 1995; Ennaciri et al., 1995b; Maacha et al., 2012): i) Co-Ni arsenide "contact" mineralisation as massive lenses located at the contact between serpentinite and quartz diorite and sometimes along the contact with the Upper Neoproterozoic volcanic rocks of the Ouarzazate supergroup; ii) Co-rich veins "cross-cutting" all lithologies; and iii) Ag-rich "stockwork" zones emplaced along the contact aureole of the quartz diorite pluton within the serpentinite. Such a contact aureole is characterised by the following mineral assemblage: prehnite-calcite-epidote-garnet-clinopyroxene, that represents a Mg-Ca±Mn metasomatic rock associated with rodingite formation (Leblanc and Lbouabi, 1988; Essarraj et al., 2005; Borisenko et al., 2014).

Five mineralisation stages have been defined at Bou Azzer (Leblanc, 1975; Ennaciri, 1995; Ennaciri et al., 1996; Ahmed et al., 2009): i) Ni-arsenide stage, mainly consisting of nickeline - NiAs and rammelsbergite - $NiAs_2$; ii) Co-arsenide stage marked by precipitation of safflorite - $(Co,Fe,Ni)As_2$, its monoclinic dimorph (*i.e.*, clinosafflorite) and skutterudite - $(Co,Ni)As_3$, sometimes associated with scarce native gold; iii) Fe-arsenide stage characterised by loellingite - $FeAs_2$; iv) sulpho-arsenide stage, consisting of gersdorffite - NiAsS, cobaltite - CoAsS and arsenopyrite – FeAsS assemblage, and v) sulphide-sulphosalt stage, with a chalcopyrite - $CuFeS_2$, sphalerite - ZnS, tennantite-tetrahedrite - $(Cu,Fe)_{12}As_4S_{13}$ - $(Cu,Fe)_{12}Sb_4S_{13}$ and molybdenite - MoS_2 assemblage, with minor brannerite - $(U,Ca,Ce)(Ti,Fe)_2O_6$ (Oberthür et al., 2009). All assemblages are associated with carbonate and/or siliceous gangue sometimes containing chlorite and talc.

The division into early "contact" mineralisation and late "cross-cutting" veins (also called "croiseurs" in French) serves as a guide for CTT's geologists and miners for both exploration and operation activities. However, no satisfying petro-structural genetic model has been proposed for the formation of the economic mineralisation so far. Hereafter based on textural and mineralogical arguments and the recognition of massive Co-Ni arsenide bodies in the core of the "contact" mineralisation, contact mineralisation is called "massive", whereas "cross-cutting" mineralisation is defined as veins or vein system. Only these two types are considered in the present study. Historically, carbonated complex shells, also called "carapace d'Ambed" and siliceous complex shells, called "Birbirite", are respectively composed of calcite and quartz, and were used in the district as major exploration guidelines on surface (Leblanc, 1975; Fanlo et al., 2015; Maacha et al., 2015).

The age of the Bou Azzer deposits is still debated. Leblanc (1975) estimated the age of Bou Azzer mineralisation during the Neoproterozoic, based on general arguments. Concordantly, Neoproterozoic to Cambrian ages were reported by Ennaciri et al. (1996; 1997) with an U/Pb age around 590-550 Ma (Ediacaran) on a single brannerite grain posterior to the Ni-and Co-rich stages.

Levresse (2001) published an $^{40}Ar/^{39}Ar$ age of 218 ± 8 Ma (upper Trias) on adularia from *Filon 7/5* linked to the silver mineralisation described by Essarraj et al. (2005). Dolansky (2007) has also provided geochronological data for brannerite from *Filon 7/5* vein system having a range of ages from 383 ± 7 Ma to 257 ± 8 Ma, i.e. Devonian to Permian. Oberthür et al. (2009) reported a large number of ages ranging from Neoproterozoic to Palaeozoic using three different dating methods: Re-Os on molybdenite, Sm-Nd on carbonates and U-Pb on brannerite. Only carbonate and brannerite gave consistent upper Carboniferous ages of 308 ± 31 Ma (Sm-Nd) and 310 ± 5 Ma (U-Pb), respectively.

3. Methods

The present study relies on new field and structural data collected during two field campaigns. Samples for this study were selected throughout the entire Bou Azzer mining from underground workings in eleven deposits, down to a depth 510 m below surface *(Taghouni, Bou Azzer Centre - Puit 3, Bou Azzer East - Puit 3 and Puit 6, Aghbar, Oumlil, Bouismass, Tamdrost, Aït Ahmane - Filon 53 and Zone D)*, seven quarries or surface outcrops *(Bou Azzer East, Quarry 52, Filon 55 surface, Filon 2, Filon 7, Filon 5 and Bou Azzer Centre)* and one surface trench *(Bou Azzer East)*(Figs. 1 and 2, Table 1, all the sites are not represented in Figure 2). The names of some of the ore bodies are in French, to keep the original names of the locations. In total, 72 polished thin sections (30 µm-thick) were prepared for studying the petro-structural features of the Bou Azzer ore deposits from 14 massive and 48 vein ore bodies. Structural data were collected from 8 massive mineralisation sites (Appendix 1.1) and 39 veins (Appendix 1.2). Direction, dip angle and dip angle orientation of each measure are indicated.

Petrography and micro-structural study were performed using optical transmitted/reflected light (TL and RL) and cathodoluminescence (CL) microscopes at the Géosciences Montpellier laboratory (University of Montpellier, France) and the Department of Earth Sciences (University of Geneva, Switzerland) to document the relationships between mineral phases and mineralised structures.

Microanalysis was carried out using a FEI Quanta FEG 100 Scanning electron microscope (SEM) and a Cameca SX100 electron probe microanalyser (EPMA) at the Service inter-regional Microsonde-Sud of Montpellier (France). Major and minor elements were measured in silicate, arsenide, sulphide and calcite grains with a beam current of 10nA and accelerating voltage of 20 keV. Nine major elements were analysed for arsenide and sulphide (standards, spectral lines, and spectrometers were as follows): Co (Co-metal, Kα, LLIF), Ni (Ni-metal, Kα, LLIF), Fe (Fe2O3, Kα, LLIF), Cu (Cu-metal, Kα, LLIF), Zn (ZnS, Kα, LLIF), Pb (PbTe, Mα, LPET), S (FeS_2, Kα, LPET), Ag (Ag-metal, Lα, LPET), Au (Au-metal, Mα, TAP), As (GaAs, Kα, LLIF). Total counting times ranged from 60 to 240 sec. The concentrations of major elements are available in Tourneur (2019). Mineral compositions (in apfu) were calculated considering a total of 3.5 atoms for the stoichiometric skutterudite and 3 oxygens for calcite.

Automated mineral analysis and textural imaging of the studied samples were performed using an FEI QEMSCAN® Quanta 650F facility at the Department of Earth Sciences, University of Geneva, Switzerland. The system is equipped with two 30 mm^2 Bruker QUANTAX light-element energy dispersive X-ray spectrometer (EDS) detectors. Analyses were conducted at high vacuum, accelerating voltage of 25 kV, and a beam current of 10 nA on carbon-coated polished thin sections. Field Image operating mode (Pirrie et al., 2004) was used for analyses. In total 221 individual fields were measured per sample, with 1500 µm per field, and point spacing of 5 µm. The standard 1000 counts per point were acquired, yielding a limit of detection of approximately 2wt% per element for mineral classifications. Measurements were performed using iMeasure v5.3.2 software and data processing using iDiscover® v5.3.2 software package. Final results consist of: i) high-quality spatially resolved and fully quantified mineralogical maps; ii) BSE images with identical resolution as the mineralogical maps; iii) X-ray element distribution maps.

Serpentine minerals were analysed by Raman spectroscopy using a Renishaw Invia spectrometer equipped with a Peltier-cooled silicon CCD detector using a 532 nm laser excitation wavelength (laserpower 30 mW, 2400 g/mm grating, spectral resolution ~ 1 cm^{-1}) at Charles Coulomb Laboratory, University of Montpellier, France. The excitation beam is provided by a Stabilite 2017 Ar^+ laser (Spectra Physics, Newport Corporation) at 514.53 nm and a power of 200 mW (resulting in ~20 mW at sample), focused on the sample surface using a x100 objective (Olympus). Two acquisitions were accumulated to provide a high-definition spectrum. To characterize the bands in the Raman spectra and identify the phases present, the online database of the French Society of Mineralogy and Crystallography and the software CrystalSleuth with the RRUFF Project database (Downs, 2006) were used (Appendix 2). Raw data were processed using LabSpec software designed for the Jobin-Yvon Horiba LabRAM instruments.

4. Structural and macroscopic study

4.1. General features

The 3D model in Figure 2 summarizes the distribution of geological units, tectonic contacts and highlights the relationships, laterally and at depth, between the two major Co-Ni-As ore body types (massive ore and veins) in the deposits from the Bou Azzer district. Figure 2 was built including field observations at the main mining sites and quarries studied (Table 1).

The ultramafic units of Bou Azzer are composed of an ancient oceanic crust (mafic dykes, layered gabbro, diabase, basalt and pillow lavas), serpentinised upper mantle and granitoid plutons (Leblanc, 1975). Serpentinite appears as discontinuous, up 10 km-long, lenses and occur always as central dome structure with north and south contacts dipping to the north and the south, respectively (Fig. 2). They are surrounded by the volcanic rocks of the upper complex in the north and by mafic

rocks in the south, certainly relicts of an ancient oceanic crust (Beraaouz et al., 2004). Most of the exploited deposits are also located south of these domes (see above), whatever their typology is (massive or veins) and along the contact between serpentinite and quartz diorite (Fig. 2).Normal fault motion was observed between serpentinite and the carbonated complex shell at the *Ambed* site (Fig. 3A). The quartz diorite intrusion crops out always south of the serpentinite (Fig. 2). Its relationship with serpentinite is not clear because the contact generally appears tectonic. However, an intrusive character has also been demonstrated, at least within the mafic rocks (Fig. 3B).

Two main structural directions exist: the N110°E-120°E general trend of the lithological units (Appendix 1.1) and the NNE crossing faults (see also Figs. 4B-D; Appendix 1.2). The massive bodies occur always parallel to the N110°E contact, except at *Bou Azzer East* (*BAE*), *Bou Azzer Centre* (*BAC*), *Bouismass* and *Aghbar* where massive mineralisation can occur along roughly NS trends (Fig. 2; Appendix 1.1). Inversely, all mineralised veins occur along the NNE faults and are high-grade only along segments in contact with serpentinite. The NNE faults do not cross the entire inlier, with one exception - the *Igherm* fault which is the longest structure affecting also the infracambrian and Cambrian units (Figs. 1 and 2). However, this is the unique fault in the area which is not mineralised, even in its part that cross-cuts the serpentinite. The vein system intersects always the massive mineralisation (*Bou Azzer Centre, Bou Azzer East – Puit 3 and Puit 6, Aghbar, Bouismass, Oumlil, Tamdrost, Filon 53* at *Aït Ahmane*). One can note that these sites only occur in the western and central parts of the district, domains where the serpentinised ultramafic mantle crops out, certainly because mostly exhumed (Leblanc, 1975; Ennaciri et al., 1997).

Near the *Taghouni* and *Bou Azzer Centre* sites, the third type of mineralisation occurs as disseminated silver and associated stockwork that are developed within the intrusive quartz diorite (Leblanc and Lbouabi, 1988) (see location in Fig. 2). Sampling is currently impossible in this area thus explaining why this type of mineralisation has not been considered in the present study.

4.2. Surface and underground observations

At surface, *serpentinite* colour is green in zones preserved from the intense carbonation and talc-alteration (Fig. 3C). Serpentinite is constantly affected by a N120°E trending foliation frequently underlined by magnetite-rich layers (Fig. 3C), but the foliation age remains unknown. These linear to dispersed magnetite-rich beds are observed in a few places like *Bou Azzer Centre* and *Bou Azzer East - Puit 3*, for example. The significance of such magnetite-rich structures will be discussed further. Close to the contact, the serpentinite texture is difficult to recognize but several locations show the presence of breccia with serpentinite fragments (Fig. 4A).

The *quartz diorite* body shows a greyish to greenish colour and feldspar and quartz grains are recognisable. Albitisation, chloritisation, epidote-rich and titanite/calcite mineral alterations affect this

rock. Disseminated ore minerals were observed but not determined at this scale. As already stated, field relationships between serpentinite and quartz diorite intrusion are not easy to define. However, several observations suggest that quartz diorite is an intrusive body (Fig. 3B). When not mineralised and occupied by massive lenses, the contact between serpentinite and quartz diorite can show three aspects: i) underlined by mafic units or dykes (Fig. 3B); ii) underlined by red levels with prehnite-calcite-epidote-garnet-clinopyroxene minerals that have been attributed to some rodingite levels supposed to represent a by-product of the serpentinisation process or maybe the effect of the contact metamorphism between serpentinite and magmatic rocks (Fig. 3D; Leblanc and Lbouabi, 1988); iii) linear with a white alteration halo (Fig. 3E). We assume that mafic dykes could be the protolith of the rodingite levels.

All structures belonging to the *vein system* intersect the whole geological units including the massive ore and may reach several hundred metres in length (Figs. 4B-D). They are filled mainly by quartz and/or carbonate, like in the *Aghbar* sector where one can observe a several metres-large left-lateral pull apart only filled by calcite and quartz (Fig. 4B). Quartz and calcite infill is ubiquitous within all vein systems at surface, either close to or far from the mineralised areas. Veins at surface comprise economic mineralisation only close to the serpentinite contact. As illustrated at *Bou Azzer Centre*, veins can exhibit two main orientations N60°E (i.e., *Filon* 7) and N10°E (i.e., *Filon* 5) (Fig. 4C). They meet together more to the south following the orientation of *Filon 7* (Fig. 4C). At the *Quarry 52* (see location on Fig. 2), massive mineralisation classically separates the serpentinite from the quartz diorite and is expressed by the numerous carbonate and siliceous complex shells characteristic for the studied area (Fig. 4E). Thus the chronology between the two systems is here confirmed because massive bodies are systematically cross-cut by veins (Fig. 4E). Numerous pockets filled by coarse-grained, euhedral calcite, are also systematically observed (Fig. 4A).

At depth, most of the massive mineralisation consists of elongated orebodies of Co-Ni-Fe arsenide, 2 to 20 metres-thick, 15 to 30 metres-long, systematically hosted in a complex quartz/carbonate gangue and observed mainly along the contact between serpentinite and quartz diorite (Figs. 5A-B). Because of its stratabound nature, no kinematic information was recordedabout the massive mineralisation. Euhedral nickeline, skutterudite and loellingite can be observed sometimes in galleries. At this scale, gangue texture is frequently massive and seems euhedral, no matter of its nature, i.e., carbonate or siliceous (Figs. 5A-B). Massive siliceous gangue is composed of quartz, chlorite, fragments of spinel and chalcopyrite. The carbonate gangue is the most abundant and shows three types of textures: i) laminated texture with carbonate/chlorite assemblage, ii) granular texture with blueish calcite (Fig. 5A) and iii) euhedral texture with white calcite and dolomite. No chronological relationships between the three textures have been determined. These textures arise some questions about the nature of the massive mineralisation protolith. Note that serpentinite fragments were frequently observed in the carbonated gangue.

The veins are exploited for Co and represent high-angle structures remarkably exposed underground. The veins are 2 to 60 cm-thick, and mineralised for about 20 metres, horizontally, only in the segments hosted within the quartz diorite. The vein system is difficult to follow inside the serpentinite where the large vein seems replaced by numerous thinner and barren fractures (Fig. 6A). In contrast with the massive mineralisation, the veins show a large variety of internal textures with dominant breccia, lamination, massive or comb-type infill (Fig. 5C). Minerals involved are quartz, Co-Fe minerals and late yellow euhedral calcite or dolomite that frequently surrounds fragments of quartz diorite and/or fragments of mineralisation (Fig. 5C). The different textures described above are equally represented in veins and their distribution results from their location: i) breccias are specifically located in pull-apart structures, ii) laminated textures characterise regular segments with homogeneous thickness and iii) comb-type infill is encountered in open-space structures. At depth also, numerous metre-scale pockets with coarse-grained euhedral carbonate infill, similar to the one observed at surface (Fig. 4A) are also frequently observed (Fig. 5D). They have the same mineralogical characteristics as the vein systems and are supposed to be formed during the same event. Kinematic indicators observed in the mineralised faults are summarised in the next section.

The different types of structures, i.e. the massive mineralisation, the vein system and associated pockets, are compared between surface outcrops and underground workings at the scale of the ore deposit as illustrated in Figure 6, in complement to Figure 2 that only shows their distribution at surface and at depth. Their main features can be summarised as follows:

- The orebody geometry is similar at surface and at depth. Both mineralisation styles show similar size (Fig. 6A) and orientation (Fig. 6B).
- Although massive mineralisation is clearly recognisable at depth, its characteristics at surface are questionable. It appears, as represented in Figure 6A, that the carbonated complex shells (carapace) or siliceous complex shells (birbirite) are the surface equivalent of the massive mineralisation at depth. However, these bodies are frequently oxidised at surface, having very dark colours.
- Mafic dykes are systematically observed at the limit between serpentinite and quartz diorite. They have the same position and orientation as the massive orebodies, but neither mineralisation, nor alteration, were observed associated with them.

4.3. Kinematic constraints

Because of the massive texture of the ore it is rather difficult to conduct kinematic observations in the lenticular orebodies. These structures strike N120°E, parallel to the Major Anti-Atlas Fault (MAAF) which cross-cut the Bou Azzer inlier and dip mostly to the NE or SW (Figs. 1, 2, 4, and 6). Inversely, the vein system exhibits abundant criteria of motion that diverge following the

vein orientation. Stereonet diagrams of Figure 6B demonstrate that veins mainly trend from N10° to N70°E with a main dipping to W or NW, respectively and values close to 60-80°.

A normal vertical motion is observed resulting in pull-apart structures (Figs. 7A-B and 8). Horizontally, both dextral and left-lateral motions are observed as indicated in the stereoplots of the Figure 6B in which dextral planes are in red whereas left-lateral ones are in black. Indeed, the veins trending close to N-S exhibit dextral sense of motion (Figs. 7C and 8) whereas the ones trending N70°E are associated with left-lateral motion (Fig. 7D). The fact that numerous textures are equally represented indicates that the vein structures were also active as fault zones and the distribution of the different textures depends on their location with respect to the fault zone. This explains why breccias are specifically located in normal motion pull-apart structures (Fig. 7D) whereas laminated textures characterise regular segments with homogeneous thickness with comb-type infill (Fig. 7A).

5. Mineralogy and microscopic texture

Differently to the five stages of the literature, three main mineralisation stages (colours in Fig. 9) have been distinguished and described below. Textural features and relative major element (Co, Ni, Fe, As, and S) abundances have been also added.

5.1. Host rocks mineralogy

The *quartz diorite* is mostly composed of albite, K-feldspar, pyroxene, apatite, quartz, oriented chloritised biotite and muscovite, rare epidote and zircon (grey in Fig. 9). Because plagioclase, pyroxene and biotite exhibit a rather subhedral forms, a hypidiomorphic granular texture is defined (Fig. 10A). Foliation is marked by white mica and secondary chlorite. Plagioclase, which has variable size, is albitic in composition (Ab# = 0.92-0.99) and occurs as euhedral to subhedral grains with typical polysynthetic twins (Tourneur, 2019). Apatite, 10 - 250 µm in size, appears as euhedral to rounded crystals showing zonation and altered rims in CL images. Near the veins, apatite is spatially associated with chlorite and loellingite, cut by k-feldspar veinlets (Fig. 10A).

The *serpentine* (grey in Fig. 9) composition is intermediate between lizardite and chrysotile, based on Raman micro-spectroscopy measurements (Appendix 2). However, lizardite is the major mineral in serpentinite, whereas fibrous chrysotile occurs as an infill in some veins close to the contact between serpentinite and massive orebodies (Fig. 10B). Serpentinite rocks are characterised by the occurrence of bastite showing the shape of pyroxene grains resisting to serpentinisation and associated pervasive carbonation (Leblanc and Lbouabi, 1988; Ahmed et al., 2005). Rammelsbergite (Ram) and nickeline (Nk1) disseminations were found within the serpentinite, close to the massive bodies (Figs. 10B-C). These minerals are the only expression of the mineralisation within the serpentinite (Fig. 10B). Scarce sulphides and sulfo-arsenides (chalcopyrite, sphalerite, galena, gersdorffite, bornite, chalcocite, digenite, Tnt-Ttr, arsenopyrite, cobaltite) can also be observed in the

serpentinite (Fig. 11A). As reported by Gahlan et al. (2006) and Fanlo et al. (2015), two types of spinels/magnetite are commonly observed in the Bou Azzer serpentinite: i) disseminated Cr-rich spinels (Fig. 10E) showing margins enriched in magnetite and ii) magnetite beds mostly located far from the massive mineralisation (Fig. 3C). Following equation (1), iron can be released from olivine during serpentinisation allowing the formation of magnetite along the border of Cr-spinel.

(1) Olivine + H_2O = Serpentine + Magnetite + H_2

$6(Mg,Fe,Ni,Co)_2SiO_4 + 7H_2O = 3(Mg,Fe,Co,Ni)_3Si_2O_5(OH)_4 + (Fe,Ni,Co)_3O_4 + H_2$

5.2. Mineralogy and mineral chemistry of the Ni-Co ore

The *massive Ni-Co orebodies* are characterised by two successive mineralisation stages:

- The early stage of Ni-arsenides (purple in Fig. 9) consists of a first generation of nickeline (Nk1, Fig. 10G) with rammelsbergite (Ram) (Figs. 10E-F and 11B-C). Note that the monoarsenide (nickeline) crystallised first followed by the diarsenide (rammelsbergite; Fig. 10G). When disseminated in serpentine, nickeline shows a higher #Co (#Co = Co / (Co+Ni+Fe)) of 0.03 than grains from the massive mineralisation where #Co is 0.005 (14 analyses; Tourneur, 2019). However, rammelsbergite shows similar #Co if the mineral is disseminated in the serpentine or occurs in the massive mineralisation (#Co=0.27 and 0.24, respectively; Tourneur, 2019).
- The second stage consists of a massive Co mineralisation (green in Fig. 9). Following the rammelsbergite deposition, the cobalt arsenide stage is characterised by the association of a first generation of cobaltite (Cob1) with small and equidimensional skutterudite (Sku1), followed by the first generation of calcite (Cal1) (Figs. 10F-G and 11B-C). Then, it is characterised by the formation of a large amount of skutterudite (Sku2) and final safflorite (Saf1; Figs. 10F-G-H). Using QEMSCAN analysis and X-ray elemental mapping, skutterudite grains show important compositional variations between Ni-rich bands and Co-rich bands, becoming progressively enriched in Co, as also observed by Gervilla et al. (2012) and Ahmed et al. (2009). The core of the grains has a Ni-skutterudite composition ($Ni_{0.75}Co_{0.25}As_{2.5}$) whereas the rims progressively acquire a more typical skutterudite composition ($Co_{0.75}Ni_{0.25}As_{2.5}$; Figs. 11B-C). ($Fe^{2+}$ + Ni^{2+}) versus Co^{2+} and As^{+} versus S^{+} show a negative correlation (Figs. 12A-B), as also noted by Dolansky (2007), Ahmed et al. (2009), Gervilla et al. (2012) and Maacha et al. (2015). Figure 12 reveals variable composition of cobalt and iron-nickel between skutterudite 1 formed in the serpentinite and skutterudite 2 of the massive mineralisation. Sku1 has high Co values

(15.4-19.5 wt% Co) while Sku2 shows lower Co content (12.1-18.0 wt% Co; Tourneur, 2019). Sku2 may therefore reflect a progressive evolution of the mineralising system as continuum process from high Co content to Ni-Fe compositions (Fig. 12B). Cob2 and Nk2 are considered as alteration minerals on Ram and Sku2 because occurring as rims around the primary rammelbersgite grains and along fractures (Figs. 9 and 13A).

Two different gangue associations (siliceous and carbonated) host the massive mineralisation (black in Fig. 9). Note that relationship between both the siliceous and carbonated gangue was not observed. The siliceous gangue is composed by a first generation of quartz (Qz1) and chlorite. It hosts Co-rich arsenides, chalcopyrite and is mostly observed in surface outcrops. The carbonated gangue is the most abundant and composed of calcite, dolomite, disseminated Cr-rich spinel and laminated chlorite associated with Co- and Fe-arsenides. The Mg-Fe-Mn diagram of carbonate which is mostly calcite in composition, integrates analyses from each structure (Fig. 12C). Calcite in the carbonated gangue shows an average of #Mn = 0.46, with a homogeneous composition with Mg and Fe (see Tourneur, 2019 for data). Carbonate composition from the surface "carapace" shows trend from Mg-rich to Mn-rich compositions (Fig. 12C; see location of the main "carapace" in Figs. 1 and 2). In the paragenetic evolution, the Ni-arsenide stage of the massive mineralisation is followed by the Co-arsenide one observed in serpentinite and in the gangue. Cal2 shows a close link with Sku2 as suggested by the crystallisation of Cal2 in the core of the growth bands of Sku2 (Fig. 13C). Disseminated Cr-rich spinel crystals with alteration halo of magnetite (Fig. 13B), are not only hosted in the serpentinite, but are also found around rammelsbergite and skutterudite 2 in the carbonated gangue (Fig. 10E). Then, Lo2 formed at the edge of safflorite (Saf2), representing what we consider as the Fe stage and also coeval with Cal2 (blue in Fig. 9, Fig. 10H). The base metal assemblage consists of sphalerite (Sp), chalcopyrite (Ccp1), arsenopyrite (Apy1), galena (Gn) and gersdorffite (Gd) in the carbonated gangue and represent the sulphide stage formed at the end of the massive mineralisation paragenesis (Fig. 9).

Veins which are intersecting massive mineralisation and quartz diorite (Fig. 6A) exhibit a complex infill with several successive stages. Infill is composed, first, of tiny to large euhedral skutterudite (Sku3) associated with an early dolomite generation (Dol1), two calcite generations (Cal3 and Cal4), comb quartz (Qz2), cobaltite (Cob2) and late calcite (Cal5) (green in Fig. 9, Figs. 11D-E and 13D). Sku3 has variable composition compared to Sku1 and Sku2 that can be easily discriminated (Fig. 12B). Figure 11F shows growth banding in skutterudite 3 with Co-, Ni- and Fe-rich zones. It is noteworthy that skutterudite of the veins contains non-negligible amount of Ni (Fig. 12B). Disseminated and oriented cobaltite (Cob3) grains with a N160°E trend were seen between comb quartz (Qz2) (Fig. 13D). Cob3 also formed along the rim of Sku3 and shows high Ni content (around

5 wt%; Fig. 11D) even though Ni-rich arsenide has never been reported in the vein system of Bou Azzer. Star-shaped safflorite (Saf2) followed by elongated crystals or also star-shaped loellingite (Lo2) are then formed as a replacement of skutterudite (Sku3), also showing variable Co and Fe content (Fig. 11F). A second generation of veinlets with euhedral adularia (Adu) crystals forms parallel to the earlier albite/quartz veins (Fig. 13E). Cal5 is enriched in Mg and Mn (Fig. 12C), with #Mn of ~ 0.66, significantly higher than those of the massive mineralisation.

The *metric-scale pockets* (Figs. 4A) exhibit open-space fillings consisting, chronologically, of quartz, carbonate and Co-Fe arsenide (Fig. 5D). They are filled by similar arsenide and sulphide mineral phases to those observed in the veins: e.g. sub-euhedral Sku3 followed by aggregates of Saf2 and Lo2 in a quartz/chlorite gangue. A comparison between loellingite in the quartz diorite, the massive mineralisation, the pockets and the veins shows that loellingite from the quartz diorite has the higher Fe content (average at 26.4 %wt. of Fe) whereas loellingite from the massive mineralisation and those from veins and pockets show lower values (respectively, average Fe contents of 17.5, 22 and 25 % wt.; see loellingite data available in Tourneur, 2019). Quartz 2 is followed by rhombohedral Cal4 associated with Cob2 and sulphides (Fig. 13F). Fragments of Lo2 are observed in the gangue of carbonate (Cal4), frequently in the middle of these structures (Fig. 11F). This calcite (here named Cal4) has a composition similar to calcite from the veins with typical high Mn content (average #Mn= 0.9; Fig. 12C). Both structures, veins and pockets, contain a late sulphide stage characterised by the formation of sphalerite, arsenopyrite, chalcopyrite and other accessory minerals (blue in Fig. 9).

5.3. Texture

Textural characteristics of the massive mineralisation, veins and pockets are indicated in the lower part of the Figure 9. The main characteristics are the following:

- Massive mineralisation exhibits complex internal texture with various aspects of the Ni-Co arsenides (Ram, Nk1, Sku1, Sku2). Rammelsbergite occurs as isolated grains in the serpentinite (Figs. 10B and 10D) and in the carbonated/siliceous gangue (Figs. 10F-G). In fact, rammelsbergite occurs as massive, isolated (Figs. 10G and 11B) and as euhedral feathery, sometimes dendritic and/or brecciated grains (Figs. 10F and 11B). Commonly, isolated rammelsbergite grains are included within massive Co-arsenide (Sku2; Figs. 10F-G and 11B). High magnification imaging and elemental mapping illustrates that euhedral feathery or dendritic rammelbersgite overgrows earlier crystals, certainly formed on previous spinel sites (Fig. 14A). In addition, Sku2, Saf2, Lo1 and Cal2 that crystallised after the first rammelsbergite generation exhibit typical euhedral shapes certainly due to an open space growth or to

replacement as discussed below (Figs. 10E-G and 13C). Optical transmitted light and cathodoluminescence microscopy revealed that the carbonated gangue hosting the arsenide shows two alternating textures: i) coarse-grained rhombohedral Cal2 with clear cleavage and twinning without visible deformation (Figs. 13C and 13G), and ii) smaller-grained with a jigsaw-like geometry, typical of brecciated domains (Fig. 13G). The occurrence of large brecciated domains of arsenide (Fig. 13G) is confirmed by the serpentinite fragments (Fig. 4A) and will be discussed below (Brecciated Massive Mineralisation, BMM).

- Rarely, massive lenses exhibit a laminated texture with alternating calcite-rich layers (Cal2) and arsenide-rich ones (Fig. 10C). These textures have been called here Laminated Massive Mineralisation (LMM) to differentiate them from the BMM (see above).
- In the core of the serpentinite, three specific features occur: i) rammelsbergite and Sku2 are commonly fractured, with a serpentine infill (Figs. 10B-C); ii) inherited fragments of serpentinite can be observed (Fig. 13H), and iii) ghosts of mesh texture of calcite are observed in the carbonated gangue (Fig. 14B).
- Open-space infill textures are characteristic for the veins. Qz3 shows comb texture formed during the opening of the veins (Figs. 13D-E). Associated to comb-quartz 3, Cob2 shows a compatible texture with a potential growth toward the vein centre (Fig. 13D). Calcite from the veins occurs also as massive rhombohedral large grains (Cal4) (Fig. 13F). Inside the veins, skutterudite exhibits fractures filled by carbonates thus illustrating syntectonic infill (Fig. 11F). Fractured apatite, chlorite and loellingite have been observed also in the quartz diorite along the vein contacts.
- Mineralised pockets are observed only inside the massive mineralisation. They show also open-space filling textures with large centimetre-scale comb-quartz (Qz3), associated with Co-Fe arsenide formed along the quartz (Fig. 13F). Cal3 of the pockets shows two types of textures: large rhombohedral texture and smaller fragmented calcite. Some fragments of Lo2 are also fractured by Cal3 and then, associated with Qz3 formation.

5.4. Alteration

Alteration of the quartz diorite is common and consists in an intense chloritisation, a complete albitisation of all feldspars, an epidote-rich alteration forming green fractures spatially associated with the massive mineralised structures and a titanite/calcite (Calc6) alteration. These features are typical of sodic-calcic alteration (Fig. 9). At the contact between the serpentinite and the quartz diorite where

no massive mineralisation is formed, a red and compact rodingite reaction was observed (see above and Fig. 3D). Serpentinite shows some talc- and carbonate- related alteration. In the massive mineralisation, Ni and Co-arsenides (Cob2, Nk2 and Gd) have been observed as secondary minerals around fractured rammelsbergite and Sku2 (Fig. 13A). Erythrine has been described by Leblanc (1975) as a supergene alteration of Co arsenide.

6. Discussion

6.1. Main results

The new contributions of our structural, textural and mineralogical study of the Bou Azzer ore system are summarized as follows:

1. The massive bodies, metre-scale in size and trending N120°E, are distributed along the contact between serpentinite and quartz diorite (Fig. 2). The vein type mineralisation is NS to N070°E trending and cross-cuts the various lithological contacts in the Bou Azzer area. The system evolves from Ni-rich-(Co-Fe) in the massive bodies to Co-rich-(Ni-Fe) mineralisation in the cross-cutting veins. In both systems, the mineralogical succession is the one established in Figure 9 and can be summarised by three mineralogical stages: i) an arsenide Ni-rich stage with rammelsbergite/nickeline developed specifically within the massive bodies, ii) an arsenide Co-rich stage forming late in the massive bodies evolution and at the beginning or as the main stage of the vein system, and iii) a final stage with Cu-Fe sulphides observed in both systems.
2. Massive mineralisation is composed by a carbonated gangue, a siliceous gangue and arsenide-rich bodies. The ore consists of decimetre-scale elongated bodies parallel to the lithological/tectonic contact between serpentine and the hanging wall lithology (quartz diorite or Precambrian volcanic rocks), whereas gangue forms lenses with complex morphology surrounding the massive bodies. The gangue texture reflects the fact that these lenses are certainly former breccia bodies with numerous residual fragments of serpentinite that have been observed at surface, underground and also at microscopic scale. Serpentinite does not occur only as fragments but also as veins and fractures (Fig. 10B) or fibrous crystals between fragmented rammelsbergite (Fig. 10C). Such textures testify of serpentinisation synchronous to the Co-rich mineralisation or corresponding to a late alteration and fracturing of the Co-rich mineralisation.
3. Textures of the massive bodies can be separated in two types:
    a. The most common texture consists of isolated lamellar rammelsbergite grains encapsulated within the paragenetic succession with, successively, Cal1, Sku1, Cob1, Ccp1 (Figs. 10F-G, 11B and 14);

b. Rarely, laminated textures are observed with alternating layers of lamellar nickeline and automorphic Cal2 (Fig. 10D). Ni-rich minerals are overgrown by calcite, cobaltite and skutterudite prior to the Fe-sulphide stage, when loellingite and chalcopyrite precipitate. The coexistence of these two textures is further used as a major criteria for constraining the formation model of the Bou Azzer mineralisation (see below).

4. The vein system exhibits internal textures resulting from a tectonically controlled mode of formation. Veins are associated with sinistral or dextral motions according to their orientation (Fig. 8) and a normal motion is systematically deduced from vertical planes of observation.
5. Formation of metre-scale pockets in the core of the massive mineralisation is attributed to the vein formation stage. These pockets are mainly characterised by large euhedral calcite that form 90% of the structures but mineralisation (quartz, skutterudite, safflorite, loellingite and cobaltite) is only found along the contacts or in central position of the pockets (Figs. 4A and 5D).
6. Within the quartz diorite, dissemination of arsenide minerals, and specifically loellingite, developed close to the vein type mineralisation. Because these minerals are fractured by K-feldspar veinlets (Fig. 10A), their formation is supposed to be earlier than the vein formation event.
7. Within the serpentinite, close or far from to the massive bodies, Cr-spinel is replaced by or transformed to magnetite (Figs. 10E and 13B; Ikenne et al., 2005; Gervilla et al., 2012; Fanlo et al., 2015). It was interpreted that in the massive parts of the orebodies, Cr-spinel is totally replaced by rammelsbergite or skutterudite.

6.2. Formation of the Bou Azzer Co-Ni-As ore mineralisation

We propose an integrated genetic model for the Co-Ni-As mineralisation at the Bou Azzer district explaining the formation of both mineralisation types (Fig. 15).

1. The geological and tectonic setting that prevails during mineralisation processes is herein constructed. We will demonstrate in the following model that this setting plays a significant role for the mode of formation and for the geometrical/morphological constraints of the various mineralisation styles in the district. Only the case of massive mineralisation developed at the contact between serpentinite and quartz diorite is presented here. It has been demonstrated that massive mineralisation occurs in the core of a gangue in which serpentinite fragments subsist. It is then concluded that a pre-existing fault zone and its associated breccia (Tourneur et al., 2019) can represent the initial stage as illustrated in Figures 15A and 15A1. Indeed, we therefore suppose an initial coexistence of laminated (mylonitic zone of the fault) and brecciated parts of the pre-existing fault. We also suppose that some

parts of the brecciated level can contain fragments of the quartz diorite and that spinel and magnetite are also present. Some domains with open space between fragments are also supposed to exist and represented in white in Figure 15A.

2. The first stage consists of hydrothermal fluid incursion which preferentially percolated along the lithological/tectonic contacts and within the highly porous brecciated area (Fig. 15B). It is unknown if the fluid arrived from the upper, lateral or lower part of the system. All possibilities are presented in Figure 15B (white arrows). During this stage, the two types of massive mineralisation were formed, i.e., the Laminated Massive Mineralisation (LMM) within mylonitic parts of the serpentinite and the Brecciated Massive Mineralisation (BMM) within the other parts. Figure 15B1 gives the microscopic details revealing that first rammelsbergite and nickeline form by replacement/transformation of the spinel fragments and magnetite concentrations. The position of Ni-minerals within the serpentinite strongly suggests that the Ni-bearing minerals replace some former Cr-spinel grains or fragments (Figs. 3C and 10E). Serpentinisation was still on-going at least during the earlier stages of this event as evidenced by the observation of serpentine veinlets and fibres that cross-cut earlier Ni-minerals such as rammelsbergite (Figs. 10B-C). Chrysotile veins also form all along the contact between serpentinite and mineralisation although this could be a later event. During the following stage (Fig. 15B2), massive mineralisation precipitates around the earlier rammelsbergite and nickeline and forms the massive bodies. Successive crystallisation of calcite, cobaltite and skutterudite surrounds the rammelsbergite lamellar crystals (Fig. 10F). It ends with the precipitation of large euhedral calcite that forms the principal carbonate gangue (Fig. 15B2). Final crystallisation of sulphides and Fe-As-rich minerals is also observed, developed within both the massive bodies and associated gangue, but also in the quartz diorite (Fig. 15B).

3. The late mineralisation stage corresponds to the emplacement of the NS to NE-SW veins (Fig. 15C). A complex infill is observed and the main mineralisation is represented by skutterudite fragments (Fig. 15C) and/or small cobaltite crystals formed in the core of vein-related comb quartz grains (Fig. 13D). Veins are structurally controlled as illustrated by their sigmoidal shape and the texture of the infill (comb quartz grains, breccia with fragments). As for the massive mineralisation, this event ended by the crystallisation of sulphides and Fe-As rich minerals both within the veins but also in the host quartz diorite. In parallel with vein formation, the development of metre-scale pockets is observed (Fig. 15C1). These pockets formed in the core of the carbonated gangue of the massive mineralisation (Fig. 5D). The pockets infill is comparable to that of the veins and exhibits, from rim to core, skutterudite 2, large euhedral quartz and carbonate (that composed 90% of the structure) and finally, safflorite, loellingite and the late Fe-rich sulphides. In our model, the pockets are developed in favour of pre-existing zones of void left between fragments of the initial breccia (see Figs. 15A and A1). The formation of these pockets, coeval to the vein system, is associated to open-space textures such as euhedral quartz and carbonate crystallisation, consistent with an on-going extensional (or transtensional) context.

Consequences of this integrated model are multiple. Two possibilities exist in order to explain the similar paragenesis: i) veins formed by remobilisation of the massive mineralisation during a late event; ii) vein and massive mineralisation are coeval and the difference is explained by a contrasting mode of formation (replacement/percolation/transformation for massive mineralisation and filling of fractures for veins). We will see in the next sections that the second hypothesis is here preferred even if uncertain. Effectively, except the Ni-rich stage that is characteristic of the early massive mineralisation, the paragenetic evolution of both structures (massive and vein mineralisation) is quite similar with successive Ni-Co-Fe arsenide, Co-Fe sulfo-arsenide and final Fe-rich sulphide stages (Fig. 9). The only divergence is textural thus indicating a different tectonic context for their formation as suggested in Figure 15. Massive orebodies were formed in situ, replacing pre-existing breccia bodies whereas vein systems result from aperture and formation of traps due to tectonics. Veins, which are only mineralised in the vicinity of the massive bodies, provide an evidence that their enrichment can result from the persistence of fluid-rock interaction. This observation demonstrates that veins can form during or immediately after the massive bodies (see below).

The hypothesis that massive mineralisation is developed as a replacement of pre-existing breccia zones explains the presently observed geometry and distribution of the different massive orebodies with a lot of small scale discontinuous deposits (Fig. 15). The consequences for exploration and exploitation strategy of the CTT mining company are significant and the necessity to account for some discontinuous and dispersed deposits is confirmed.

6.3. Mineralogical evolution

Because the mineralogical evolution found within both systems is similar except the presence of Ni-minerals only within the massive orebodies, we propose that, even if massive bodies are formed first, continuity may exist between the processes responsible for the formation of massive and vein mineralisation in different tectonic context. The massive mineralisation could be formed by a replacement of the brecciated contact zones between serpentinite, quartz diorite and Precambrian volcanic rocks due to hydrothermal fluids circulation. Vein system is coeval and formed by remobilisation of the massive mineralisation specifically because they are mineralised only at their contact and certainly because necessary conditions prevailed to allow the precipitation of metal-bearing fluid. The fact that late large-scale fault (the Igherm Fault, Fig.1C) cross-cutting the entire Bou Azzer domain is not mineralised confirms the close relationships, at least in time between the two systems (see above). This may confirm that P-T conditions necessary for fluid-rock interactions were still preserved during the formation of the vein system, so certainly during or later to the massive ore formation. Indeed, if later, veins would have cross-cut the Cambrian units.

Each structure shows similar features that explain the hydrothermal control of mineralisation by the circulation of hot brines along lithological contacts (massive bodies) or faults (veins system)(e.g. Ennaciri et al., 1995; Essarraj et al., 2005; Ahmed et al., 2009; Burisch et al., 2017; Ikenne et al., 2020; Hajar et al., 2020):

i) Ni-Co massive mineralisation is supposed to develop by replacement/transformation of spinel/magnetite grains of the serpentinite host rock as illustrated in Figures 10E and 13B and already suggested in the literature (Gervilla et al., 2012; Fanlo et al., 2015);

ii) the carbonated gangue close to the massive mineralisation is interpreted as a serpentinite breccia transformed by a hydrothermal fluid along the contact between the quartz diorite, Precambrian volcanic rocks and serpentinite. The occurrence of preserved serpentinite fragments (Fig. 13G), spinel fragments (Fig. 13B) and maybe ghost mesh texture entirely overprinted by calcite (Figs. 14B-C) provide the basis of this interpretation;

iii) an extensional context with low-angle detachment can lead to the formation of open-space between fragments of the brecciated zones. Large scale pockets filled by euhedral minerals indicate open space crystallisation, consistent with that expected within a brecciated extensional environment;

Hydrothermal leaching of the host rocks seems at the origin of the remobilisation of the economic elements. This has been texturally demonstrated here but would need a confirmation by mass balance calculations. However, we can suppose that Ni and Co have their origin mainly from the ultramafic rocks (Laubier et al., 2014), Fe from the quartz diorite or oxides and base metal elements from meta-oceanic rocks or serpentinite (Leblanc and Fischer, 1990; Alt and Shanks, 1998). Also, the source of such a large amount of arsenic necessary to form the Bou Azzer Co-Ni-As mineralisation remains questionable. Smedley and Kinniburgh (2002) and Burisch et al. (2017) made a compilation about the source of arsenic in minerals and rocks (Appendix 3). Arsenic can be concentrated within various types of rocks and minerals such as Fe-oxide, apatite and magnetite but also in ultramafic, sedimentary or intermediate igneous rocks (diorite, granodiorite). Following the authors, fibrous magnetite (concentration up to 400 ppm), magnetite disseminated grains or veins (< 20 ppm), sulphide in serpentinite (50 to 1000 ppm), Neoproterozoic granitoid intrusions (< 10 to ~ 25 ppm), serpentinite (200 ppm), and volcanic rocks of the Ouarzazate supergroup (100 to 300 ppm) (Leblanc, 1975; Gahlan et al., 2006; Leblanc and Fischer, 1990; Beraaouz et al., 2004; Hattori et al., 2005; Leblanc and Billaud, 1982, respectively) are good candidates as source rocks. However, principally because the excess of As is expressed within mineralisation that occurs as a replacement/transformation of relictic Cr-spinel hosted in serpentinite fragments (this study) and because it has been also demonstrated that Ni and Co-rich arsenide minerals developed as a

788 replacement of relictic Cr-spinel partially bordered by magnetite (Fig. 13b; Gervilla et al., 2012; Fanlo
789 et al., 2015), the serpentinite and all accessory minerals inside are the best candidates as source for As
790 at Bou Azzer, even if the apatite of the quartz diorite cannot be excluded.
791

792 **6.4. Tectonic and geodynamic setting**

793 One of the main results of our study is the establishment of an initial context that can explain
794 the specificity of the Bou Azzer mineralisation. Because of the preservation of numerous serpentinite
795 fragments, the initial breccia certainly formed along detachment fault contact between serpentinite
796 and quartz diorite or Precambrian volcanic rocks (i.e., Fig. 3A). Indeed, we assume that previously to
797 the mineralisation, brecciated zones with subsequent permeability may form in domains that were
798 later transformed into massive orebodies and associated gangue mineralisation. Because these
799 breccias occur as elongated pluri-metric-scale lenses systematically developed at the contact between
800 the serpentinite and other units (mainly quartz diorite), we suggest they can correspond to some pre-
801 existing fault-related polymictic sedimentary breccias developed along fault slope as already
802 suggested in the case of the French Pyrenees (Clerc et al., 2012). Indeed, these breccia outcrops can
803 be compared to the famous ophicalcite lithologies defined as brecciated and fractured peridotites with
804 a carbonate matrix (Clerc et al., 2012), as illustrated in Figure 16. We also propose that the siliceous
805 gangue was formed following similar processes but within parts dominated by quartz diorite
806 fragments. But this hypothesis has not been followed by thorough analysis. In the case of Bou Azzer,
807 it is then proposed that the location in which massive mineralisation was developed can be defined as
808 tectonic contacts. LMM and BMM types of mineralisation are then formed during the same event, but
809 depending on the position within the fault context and on the initial texture, as illustrated in Figures
810 15 and 16.

811 The nature of the fault and consequently the type of context remains questionable. It is
812 noteworthy that ophicalcite has been described mainly within extensional domains and specifically
813 within area where mantle exhumation took place (Hölker et al., 2003, Lagabrielle and Bodinier, 2008;
814 Caby, 2014). These rocks are finally intimately associated with the recent concept of a mantle
815 exhumation within extremely thinned continental margin and/or Oceanic Continent Transition (OCT).
816 The nature of the tectonic contacts and the geodynamic setting of the Bou Azzer serpentinite
817 exhumation are not subject of this study and will be re-addressed in a paper in preparation (Chauvet et
818 al., in prep.). However, it can be suggested, as a preliminary idea, that such hyper extension can be
819 developed in a back-arc position with respect to the geodynamic model proposed by Triantafyllou et
820 al. (2018). This model suggested that a north-dipping subduction may form the Tichibanine,
821 Tazigzaout and Bougmane arcs (see location in Fig. 1c), intensively affected by subsequent
822 deformation in response to the N-S trending compression. However, the lack of intensive deformation

in the Bou Azzer parts where serpentinite crops out may suggest that such areas can be rather affected by hyper-extension that can explain the mantle exhumation helped by normal faulting with a deformation extremely located close to the contact (Fig. 16) (Ishii et al., 1992; Jolivet et al., 2018).

The quartz-diorite body formation remains a riddle. In this study, we argue for intrusive relationships (Figs. 3B and 4A). Two alternatives can be advanced. First, the quartz diorite can be the result of the north-dipping subduction proposed by Triantafyllou et al. (2018). Therefore, its location in the core of a hyper-extended rift more to the north is justified. Another solution would be that the quartz diorite resulted from the intrinsic exhumation process as predicted by Manatschal (2004) as a character of rifted margin in which mantle exhume to the sea floor.

Although the formation of massive mineralisation can be considered as the result of replacement/transformation processes, the vein system appears clearly dependent on the tectonics. Syn-tectonic infill textures associated with transcurrent/normal faulting (Fig. 7) are the main arguments. NS dextral and NE sinistral conjugated vein systems are consistent with a N030°E shortening direction, certainly associated with a vertical component explaining the systematic normal motion (Fig. 8). Pull-apart structures are the most abundant. These motions are the ones that are coeval with vein/fault formation because controlling their infill. Transtension is suggested because of the systematic association between wrench motion and normal ones. Such a NE-SW shortening direction during transtensive tectonics has been already suggested by Tuduri et al. (2018a), and particularly as controlling the final mineralisation stage in various deposits of the Jbel Saghro, during the upper complex formation. Several Au-Ag occurrences of the central Anti-Atlas of Morocco, i.e., the *Thaghassa* intrusion-related gold deposit (Tuduri et al., 2018b), the *Qal'at Mgouna*, and *Zone des Dykes* gold indexes and the second stage of the *Imiter* silver mine are the main examples (Tuduri et al., 2018a).

The formation of the geodic textures in metre-scale pockets remains also questionable. The mineralogical argument suggests that there are coeval with the vein system (this study). They do not show any argument for structural control but they are clearly post–dating the massive mineralisation based on cross-cutting relationships. Such an open space environment, as already suggested by Ennaciri et al. (1997), is consistent with the transtensional character of the second mineralising event as discussed above. Moreover, it can be suggested that the metre-scale pockets can finally re-use and benefit from the high porosity and large open space that can exist in the slope-related breccia lenses that served as a trap for the massive mineralisation. Such open spaces are represented in the schematic petro-structural evolution of the deposit (Fig. 15).

Leblanc (1975) estimated the age of Bou Azzer mineralisation to be Neoproterozoic, based on general arguments. Palaeozoic age was proposed by Essarraj et al. (2005) explaining that the Bou Azzer district was formed by basinal brines circulation occurring during the early stage of the Atlantic rifting. Inversely, Oberthür et al. (2009), that obtained Hercynian ages, proposed a possible reworking of older minerals. Applying the indirect data obtained in this study and specifically the fact that both

types of mineralisation seem to develop in continuity (mineralogical arguments), it is strongly suggested here that the Bou Azzer mineralisation was formed during the same period of time. The tectonic context that prevailed during vein formation, defined by conjugate NS dextral and NE left-lateral normal veins (Fig. 8), seems similar to the second transtension stage that has been defined and demonstrated recently by Tuduri et al. (2018a) as a major tectonic event that affected the Jbel Saghro, more to the N-NE (see above). In that case, the formation of earlier massive mineralisation could have taken place only during the early Neoproterozoic, fact that is consistent with the intervention of hyper-extension in response to the north-directed subduction suspected southward of the Bou Azzer district (Triantafyllou et al., 2016).

With such a hypothesis, the numerous young ages obtained in this area could be related to remobilisation processes during the Hercynian orogeny. In fact, the large spectrum of ages between 310 to 70 Ma presents an evidence of improper duress of dating, certainly in favour of unsatisfying results. Because the Hercynian hypothesis is frequently advanced within the entire Anti-Atlas by a number of authors (see discussion in Levresse et al., 2017) one can question about the numerous geochronological data obtained within the entire Anti-Atlas (see also Essarraj et al., 2016) while no structure can be clearly related to these Hercynian or maybe younger orogenesis. A recent article underlined fault reactivation during Variscan and Alpine cycles but this appears no sufficient to explain such an abundance of absolute ages. As the entire Anti-Atlas was buried under a thick marine sedimentary cover from Middle Cambrian to Lower Devonian (Soulaimani et al., 2014), we question if such a landfill can be at the origin of age rejuvenation and consequently of the numerous young ages reported in this area (Caby, personal communication).

6.5. Deposit classification and consequences for exploration strategy

The Bou Azzer district has been considered recently as a five-element veins type deposit by Markl et al. (2016) and Burisch et al. (2017). The five-element veins deposits (Bi-Co-Ni-Ag±U) have open-space infill characterised by two specific mineral associations: Co-Ni sulphides and Co-Ni arsenides, with or without dendritic to wire-like texture of native elements like silver, arsenic and bismuth in a carbonate gangue. They are related to hydrothermal processes affecting various sedimentary, igneous or metamorphic rocks. Indeed, it is clear that deposits of the Bou Azzer district and particularly the Ag-rich *Tizi* deposit (see location in Fig. 2) can be easily compared to the five-element veins classification as already suggested. However, a lot of questions subsist. First, although the late Ag-Hg stage clearly takes place after the Co-As and base metal stages (Leblanc and Lbouabi, 1988; Ennaciri et al., 1997; Essarraj et al., 2005), the age of their formation, the genetic link with the Bou Azzer Co-Ni-As mineralisation and the mode of formation remain uncertain. Second, the five-element veins classification does not provide a satisfying model of formation although a few genetic

theories have been proposed by Kissin (1992); one of them related to a magmatic-hydrothermal concept occurring in the continental crust and associated with extensional tectonics. Indeed, this unsatisfying situation justifies the new and original model of formation discussed above in this work. Although the model of formation proposed in this study brings significant information regarding the distribution and the characteristics of the numerous and various Ni-Co-As orebodies of the whole Bou Azzer district, a large uncertainty subsists about the processes of metal concentration specifically for the massive orebodies. Our study provides additional evidence that at least the massive part of the mineralisation was formed by in-situ transformation of existing minerals such as spinel and magnetite. We do not success in demonstrating if this transformation is dominated by replacement, overgrowth, remobilisation or dissolution-precipitation process although recent studies favours replacement (e.g., Gervilla et al., 2012; Fanlo et al., 2015). The model of formation of the Bou Azzer deposits may resemble to the replacement processes highlighted in some models of volcanic-hosted massive sulphide (VHMS) formation (Aerden, 1993; Relvas et al., 2000; Doyle and Allen, 2003), except that relationship with the main metamorphism event is not demonstrated at Bou Azzer. Gervilla et al. (2012) mentioned it for the case of the Co-Ni-As Bou Azzer district. In spite of the nature of the Co-Ni-As mineralisation and the lack of abundant polymetallic sulphides, we can tentatively suggest that the Bou Azzer district may correspond to a model close to the one of the VHMS but with formation of arsenides rather than sulphides. The drastic divergence between the two end-members, i.e. sulphide versus arsenide, can be explained by the implication of the particular association between ultramafic rocks (serpentinite) and plutonic (quartz diorite) in the second case, i.e., the Bou Azzer case. Indeed, we propose that the Bou Azzer district is related to Massive Arsenide deposit instead of a Massive Sulphide one. The term “Volcanic Hosted” can be replaced, in this case, by “Serpentinite Hosted” and the acronym used could be SHMA, Serpentinite-Hosted Massive Arsenide. In this model, the distribution of the previous breccia lenses is the most important factor in order to explain the distribution of massive mineralisation ore bodies. This may explain why the Bou Azzer district is composed of numerous, isolated, small-size, orebodies rather than a continuous and regular mineralisation.

7. Conclusion

Based on new field, structural, textural, petro-structural and mineralogical arguments, we propose a new genetic model for the famous Bou Azzer Co-Ni-As (-Au-Ag) district that explains the formation of the two types of mineralisation. Because of the particular significance of the serpentine and the original arsenide-rich mineralogy, we propose to call this type of deposit SHMA (Serpentinite-Hosted Massive Arsenides). In this hypothesis, several lines of evidence argue for this new classification. Because the massive part of the deposit is formed by circulation of hydrothermal fluids across a serpentinite breccia formed during tectonic exhumation along low-angle extensional detachment, the model of formation is similar to the one of VHMS except the fact that “basement and

source" rocks are serpentinite rather than volcanic or oceanic crust. The significance of replacement processes is an additional argument for explaining their mode of formation. The presence of intrusive rocks and exhumed mantle transformed to serpentinite (source for Ni and Co) is essential for the formation of this deposit type. The nature of the low-angle extensional contact is not, for the moment, entirely demonstrated. Preliminary observations (Fig. 3A) argue for general extensional setting (Tourneur et al., 2019).

Acknowledgements MANAGEM and CTT mining companies are acknowledged for their financial supports during field works and access to the mine sites. MANAGEM provide entire field trip coasts for J.T., K.K. and S.S whereas part of the field trip of E.T. and A.C. are provided by the European program MEDYNA. Part of the laboratory works was supported by the Tellus Program of CNRS/INSU and the PHC Campus Germaine de Steel, other part by particular funds provided by A.C. Christophe Nevado and Doriane Delmas are particularly acknowledged for their meticulous works for thin sections preparation. Constructive comments by D. Aerden and four anonymous reviewers are gratefully appreciated.

References

Admou, A., Razin, Ph., Egal, E., Youbi., N., Soulaimani, A., Blein, O., Chèvremont, Ph., Gasquet, D., Barbanson, L., Bouabdelli, M., Anzar-Conseil, 2013. Notice explicative, carte geol. Maroc (1/50000). Notes et Mémoires Serv. Géol. Maroc N°533bis, MEM/BRGM.

Aerden, D.G.A.M., 1993. Formation of Massive Sulfide Lenses by Replacement of Folds: The Hercules Pb-Zn Mine, Tasmania. Econ. Geol., 88, 377-396.

Ahmed A.H., Arai, S., Abdel-Aziz; Y.M., Rahimi, A., 2005. Spinel composition as a petrogenetic indicator of the mantle section in the Neoproterozoic Bou Azzer ophiolite, Anti-Atlas, Morocco. Precam. Res., 138, 225–234.

Ahmed, A.H., Arai, S., Ikenne, M., 2009. Mineralogy and paragenesis of the Co-Ni arsenides ores of Bou Azzer, Anti-Atlas, Morocco. Econ. Geol., 104, 249-266.

Alt, J.C., 1995. Subseafloor processes in mid-ocean ridge hydrothermal systems. Seafloor Hydrothermal Systems. Physical, Chemical, Biological, and Geological Interactions, pp. 85-114

Alt, J.C., Laverne, C., Vanko, D.A., Tartarotti, P., Teagle, D.A., Bach, W., Zuleger, E., Erzinger, J., Honnorez, I., Pezard, P.A., 1996. Hydrothermal alteration of a section of upper oceanic crust in the eastern equatorial Pacific: A synthesis of results from Site 504 (DSDP Legs 69, 70, and 83, and ODP Legs 111, 137, 140, and 148). Proceedings of the Ocean Drilling Program: Scientific Results, 148, 417-434.

968 Alt, J.C., Shanks, W., 1998. Sulfur in serpentinized oceanic peridotites: Serpentinization processes
969 and microbial sulfate reduction. J. Geophys. Res., 103, 9917–9929. doi:10.1029/98JB00576
970 Arndt, N.T., Lesher, C.M., Czamanske, G.K., 2005. Mantle-derived magmas and magmatic Ni-Cu-
971 (PGE) deposits, In: Hedenquist, J.W., Thompson, J.F.H., Goldfarb, R.J., Richard, J.P. (Eds.),
972 Economic Geology, 100th Anniversary Volume, pp. 5-23.
973 Barbey, P., Oberli, F., Burg, J.P., Nachit, H., Pons, J., Meier, M., 2004. The Paleoproterozoic in
974 western Anti-Atlas (Morocco): A clarification. J. African Earth Sci, 39, 239-245.
975 Bastin, E.S., 1939. The nickel-cobalt-native silver ore type. Econ. Geol., 34, 1-40.
976 Beraaouz, E. H., Ikenne, M., Mortaji, A., Madi, A., Lahmam, M., Gasquet, D., 2004. Neoproterozoic
977 granitoids associated with the Bou-Azzer ophiolitic melange (Anti-Atlas, Morocco): Evidence
978 of adakitic magmatism in an arc segment at the NW edge of the West-African craton. J. African
979 Earth Sci., 39, 285-293.
980 Blein, O., Baudin, T., Chèvremont, P., Soulaimani, A., Admou, H., Gasquet, P., Cocherie, A., Egal,
981 E., Youbi, N., Razin, P., Bouabdelli, M., Gombert, P., 2014. Geochronological constraints on
982 the polycyclic magmatism in the Bou Azzer-El Graara inlier (Central Anti-Atlas Morocco): J.
983 African Earth Sci., 99, 287-306.
984 Bodinier, J.L., Dupuy, C., Dostal, J., 1984. Geochemistry of Precambrian ophiolites from Bou Azzer,
985 Morocco. Contrib. Miner. Petrol., 87, 43-50.
986 Boillot, G., Recq, M., Winterer, E.L., Meyer, A.W., Applegate, J., Baltuck, M., Bergen, J.A., Comas,
987 M.C., Davies, T.A., Dunham, K., Evans, C.A., Girardeau, J., Goldberg, G., Haggerty, J., Jansa,
988 L.F., Johnson, J.A., Kasahara, J., Loreau, J.P., Luna-Sierra, E., Moullade, M., Ogg, J., Sarti, M.,
989 Thurow, J., Williamson, M., 1987. Tectonic denudation of the upper mantle along passive
990 margins: a model based on drilling results (ODP leg 103, western Galicia margin, Spain).
991 Tectonophysics, 132, 335-342.
992 Borisenko, A.S., Lebedev, V.I., Borovikov, A.A., Pavlova, G.G., Kalinin, Y.A., Nevol'ko, P.A.,
993 Kostin, A.V., 2014. Forming Conditions and Age of Native Silver Deposits in Anti-Atlas
994 (Morocco). Doklady Earth Sciences, 456, 663–666.
995 Bouchta, R., Boyer, F., Routhier, P., Saadi, M., Salem, M., 1977. L'aire cuprifère de l'Anti-Atlas
996 (Maroc) : Permanence et arêtes riches. C. R. Acad. Sc. Paris, 284, 503-506.
997 Bourque, H., Barbanson, L., Sizaret, S., Branquet, Y., Ramboz, C., 2014. Copper Mineralisation in
998 Adoudounian Cover of the Bou Azzer-El Graara (Anti Atlas, Morocco): Tectono-Stratigraphic
999 Controls. Mineral Resources in a Sustainable Word, 4, 1575–1578.
1000 Bousquet, R., El Mamoun, R., Saddiqi, O., Goffé, B., Möller, A., Madi, A., 2008. Mélanges and
1001 ophiolites during the Pan-African orogeny: the case of the Bou-Azzer ophiolite suite
1002 (Morocco). Geological Society, London, Special Publications, 297, 233-247.

1003 Burisch, M., Gerdes, A., Walter, B., Neumann, U., Fettel, M., Markl, G., 2017. Methane and the
1004 origin of five-element veins: Mineralogy, age, fluid inclusion chemistry and ore forming
1005 processes in the Odenwald, SW Germany. Ore Geol. Rev., 81, 42-61.
1006 Burkhard, M., Caritg, S., Helg, U., Robert-Charrue, C., Soulaimani, A., 2006. Tectonics of the Anti-
1007 Atlas of Morocco. C. R. Geosciences, 338, 11-24.
1008 Butt, C.R.M., Cluzel, D., 2013. Nickel Laterite Ore Deposits: Weathered Serpentinites. Elements, 9,
1009 123-128.
1010 Caby, R., 2014. Nature and evolution of Neoproterozoic ocean-continent transition: Evidence from
1011 the passive margin of the West African craton in NE Mali. J. African Earth Sci, 91, 1-11.
1012 Cailteux, J.L.H., Kampunzu, A.B., Lerouge, C., Kaputo, A.K., Milesi, J.P., 2005. Genesis of
1013 sediment-hosted stratiform copper–cobalt deposits, central African Copperbelt. J. African Earth
1014 Sci., 42, 134-158.
1015 Clerc, C., Lagabrielle, Y., Neumaier, M. Reynaud, J.Y., Saint Blanquat, M., 2012. Exhumation of
1016 subcontinental mantle rocks: evidence from ultramafic-bearing clastic deposits nearby the
1017 Lherz peridotite body, French pyrenees. Bull. Soc. Géol. Fr., 5, 443-459.
1018 Chauvet, A., Tourneur, E., Paquez, C., Bodinier, J.L., Ennaciri, A., in preparation. A new geodynamic
1019 vision of the Bou Azzer - El Graara inlier, Anti-Atlas, Morocco. Obduction versus hyper
1020 extension model. To be submitted in Journal of Structural Geology.
1021 Choubert, G., 1945. Sur le Précambrien marocain. C. R. Acad. Sci Paris, 221, 249-251.
1022 Choubert, G., 1963. Histoire géologique du Précambrien de l'Anti-Atlas. Notes Mem. Serv. Géol.
1023 Maroc, 162, 352 p.
1024 Choubert, G., Faure-Muret, A., 1980. Anti-atlas (Morocco). Earth-Science Reviews, 16, 87-113
1025 Clauer, N., 1976. Géochimie isotopique du strontium des milieux sédimentaires – application à la
1026 géochronologie de la couverture du craton Ouest-Africain. Sci. Géol. Mém., 45, 256 p.
1027 Coltat, R., Branquet, Y., Gautier, P., Campos Rodriguez, H., Poujol, M., Pelleter, E., McClenaghan,
1028 S., Manatschal, G. and Boulvais, P., 2019. Unravelling the root zone of ultramafic-hosted black
1029 smokers-like hydrothermalism from an Alpine analog. Terra Nova, 31(6), 549-561.
1030 Dolansky, L.M., 2007. Controls on the genesis of hydrothermal cobalt mineralisation: Insights from
1031 the mineralogy and geochemistry of the Bou Azzer deposits, Morocco. Unpublished M.Sc.
1032 thesis, Montreal, Canada, McGill University, 192 p.
1033 Downs, R.T., 2006. The RRUFF Project: an integrated study of the chemistry, crystallography,
1034 Raman and infrared spectroscopy of minerals. Program and Abstracts of the 19th General
1035 Meeting of the International Mineralogical Association in Kobe, Japan. O03-13.
1036 Doyle, M.G., Allen, R.L., 2003. Subsea-floor replacement in volcanic-hosted massive sulfide
1037 deposits. Ore Geol. Rev., 23, 183-222

1038 El Ghorfi, M., Oberthür, T., Lüders, V., El Boukhari, A., Melcher, F., Maacha, L., Ziadi, R.,
1039 Baoutoul, H., 2006. Gold–palladium mineralisation at Bleïda Far West, Bou Azzer–El Graara
1040 Inlier, Anti-Atlas, Morocco. Miner. Dep., 41, 549-564.
1041 El Hadi, H., Simancas, J.F., Martínez-Poyatos, D., Azor, A., Tahiri, A., Montero, P., Fanning, C.M.,
1042 Bea, F., González-Lodeiro, F., 2010. Structural and geochronological constraints on the
1043 evolution of the Bou Azzer Neoproterozoic ophiolite (Anti-Atlas, Morocco). Precam. Res., 182,
1044 1-14.
1045 Ennaciri, A., 1995. Contribution à l'étude du district à Co, As, (Ni, Au, Ag) de Bou Azzer, Anti-Atlas
1046 (Maroc). Données minéralogiques et géochimiques : Etude des inclusions fluides. Unpublished
1047 M.Sc. thesis, University of Orléans, 238 p.
1048 Ennaciri, A., Barhanson, L., Touray, J.C., 1995. Mineralised hydrothermal solution cavities in the Co-
1049 As Aït Ahmane mine (Bou Azzer, Morocco). Miner. Dep., 30, 75- 77.
1050 Ennaciri, A., Barbanson, L., Lancelot, J., Touray, J.C., 1996. Distribution et âge de mise en place des
1051 minéralisations aurifères du district de Bou Azzer) (Anti-Atlas, Maroc): Abstract, Réunion des
1052 Sciences de la Terre, 16th, Orléans, p. 153.
1053 Ennaciri, A., Barbanson, L., Touray, J. C., 1997. Brine inclusions from the Co-As(Au) Bou Azzer
1054 district, Anti-Atlas mountains, Morocco. Econ. Geol., 92, 360-367.
1055 Ennih, N., Liégeois, J., 2001. The Moroccan Anti-Atlas : the West African craton passive margin with
1056 limited Pan-African activity. Implications for the northern limit of the craton. Precam. Res.,
1057 112, 289–302.
1058 Essarraj, S., Boiron, M.C., Cathelineau, M., Banks, D.A., Benharref, M., 2005. Penetration of surface-
1059 evaporated brines into the Proterozoic basement and deposition of Co and Ag at Bou Azzer
1060 (Morocco): Evidence from fluid inclusions. J. African Earth Sci, 41, 25-39.
1061 Essarraj, S., Boiron, M.C., Cathelineau, M., Tarantola, A., Leisen, M., Boulvais, P., Maacha, L., 2016.
1062 Basinal brines at the origin of the Imiter Ag-Hg deposit (Anti-Atlas, Morocco): Evidence from
1063 LA-ICP-MS data on fluid inclusions, halogen signatures, and stable isotopes (H, C, O). Econ.
1064 Geol., 111, 1753-1781.
1065 Fanlo, I., Gervilla, F., Colás, V., Subías, I., 2015. Zn-, Mn- and Co-rich chromian spinels from the
1066 Bou-Azzer mining district (Morocco): Constraints on their relationship with the mineralising
1067 process. Ore Geol. Rev., 71, 82–98. https://doi.org/10.1016/j.oregeorev.2015.05.006
1068 Freyssinet, P., Butt, C.R.M., Morris, R.C., Piantone, P., 2005. Ore-forming processes related to
1069 lateritic weathering. In: Hedenquist, J.W., Thompson, J.F.H., Goldfarb, R.J., Richard, J.P.
1070 (Eds.), Economic Geology 100th Anniversary Volume. Society of Economic Geologists, Inc,
1071 Littleton, Colourado, pp. 681-722.
1072 Gahlan, H., Arai, S., Ahmed, A.H., Ishida, Y., Abdel-Aziz, Y.M., Rahimi, A., 2006. Origin of
1073 magnetite veins in serpentinite from the Late Protero- zoic Bou-Azzer ophiolite, Anti-Atlas,

Morocco: An implication for mobility of iron during serpentinisation. J. African Earth Sci., 46, 318–330.

Gasquet, D., Levresse, G., Cheilletz, A., Azizi-Samir, M.R., Mouttaqi, A., 2005. Contribution to a geodynamic reconstruction of the Anti-Atlas (Morocco) during Pan-African times with the emphasis on inversion tectonics and metallogenic activity at the Precambrian-Cambrian transition. Precam. Res., 140, 157-182.

Gervilla, F., Fanlo, I., Colas, V., Subias, I., 2012. Mineral composition and phases relation of Ni – Co – Fe arsenides ores from the Aghbar mine, Bou Azzer, Morocco. The Canadian Mineralogist, 50, 447-470.

Hajar, Z., Gervilla, F., Fanlo, I., Jiménez, J.M.G., Ilmen, S., 2020, Formation of serpentinite-hosted, Fe-rich arsenide ores at the latest stage of mineralization of the Bou-Azzer mining district (Morocco). Ore Geol. Rev. In Press.

Hattori, K., Takahashi, Y., Guillot, S., Johanson, B., 2005. Occurrence of arsenic (V) in forearc mantle serpentinites based on X-ray absorption spectroscopy study. Geochim. Cosmoschim. Acta, 69, 5585-5596

Hefferan, K.P., Admou, H., Karson, J.A., Saquaque, A., 2000. Anti-Atlas (Morocco) role in Neoproterozoic Western Gondwana reconstruction. Precam. Res., 103, 89-96.

Hein, J.R., Koschinsky, A., 2014. Deep-Ocean Ferromanganese Crusts and Nodules. In: Holland, H.D., Turekian, K.K. (Eds.), Treatise on Geochemistry (Second Edition), volume 13, chapter 11, Elsevier, Oxford, pp. 273-291.

Hitzman, M.W., Broughton, D., Selley, D., Woodhead, J., Wood, D., Bull, S., 2012. The Central African Copperbelt: Diverse stratigraphic, structural, and temporal settings in the world's largest sedimentary copper district. In: Hedenquist, J.W., Harris, M., Camus, F. (Eds.), Geology and Genesis of Major Copper Deposits and Districts of the World: A Tribute to Richard H. Sillitoe. Society of Economic Geologists, Littleton, Co, pp. 487-514.

Hollard, H., Choubert, G., Bronner, G., Marchand, J., Sougy, J., 1985. Carte géologique du Maroc, échelle: 1/1.000.000. Notes et Mémoires du Service Géologique du Maroc, 260 p.

Hölker, A., Manatschal. G., Holliger, K., Bernoulli, D., 2003. Tectonic nature and seismic response of top-basement det achment faults in magma-poor rifted margins. Tectonics, 22, 4, 1035.

Ikenne, M., Madi, A., Gasquet, D., Cheilletz, A., Hilal, R., Mortaji, A., Mhaili, E., 2005. Petrogenetic significance of podiform chromitites from the Neoproterozoic ophiolitic complex of Bou Azzer (Anti-Atlas, Morocco). Africa Geosci. Rev., 12 (2), 131-143.

Ikenne, M., Souhassou, M., Saintilan, N.J., Karfal, A., El Hassani, A., Moundi, Y., Ousbih, M., Ezzghoudi, M., Zouhir, M., Maacha, L., 2020. Cobalt-Nickel-Copper arsenide, sulpharsenide and sulphide mineralisation in the Bou Azzer window, Anti-Atlas, Morocco: One century of multi-disciplinary and geological investigations, mineral exploration and mining. Geological Society, London, Special Publications, 502. https://doi.org/10.1144/SP502=2019-132

1111 Inglis, J.D., Lemos, R.S.D., Samson, S.D., Admou, H., 2005. Geochronological Constraints on Late
1112 Precambrian Intrusion, Metamorphism and Tectonism in the Anti-Atlas Mountains. The Journal
1113 of Geol., 113, 439-450.
1114 Ishii, T., Robinson, P.T., Maekawa, H., Fiske, R., 1992. Petrological studies of peridotites from
1115 diapiric serpentinite seamounts in the Izu–Ogasawara–Mariana Forearc, Leg 125. In: Fryer, P.,
1116 Pearce, J.A., Stokking, L.B., et al. (Eds.), Proceeding of the Ocean Drilling Program, Scientific
1117 Results, 125, 445-485.
1118 Jolivet, L., Menant, A., Clerc, C., Sternai, P., Bellahsen, N., Leroy, S., Pik, R., Stab, M., Faccenna, C.,
1119 Gorini, C., 2018. Extensional crustal tectonics and crust-mantle coupling, a view from the
1120 geological record. Earth-Science Rev., 185, 1187-1209.
1121 Kissin, S.A., 1992. Five-element (Ni-Co-As-Ag-Bi) veins: Geosciences Canada, 19, 113-124.
1122 Kreissl, S., Gerdes, A., Walter, B., Neumann, U., Wenzel, T., Markl, G., 2018. Reconstruction of a >
1123 200 Ma multi-stage "five-element" Bi-Co-Ni-Fe-As-S system in the Pennininc Alps,
1124 Switzerland. Ore Geol. Rev., 95, 746-788.
1125 Lagabrielle, Y., Bodinier, J.L., 2008. Submarine reworking of exhumed subcontinental mantle rocks:
1126 Field evidence from the Lherz peridotites, French Pyrenees. Terra Nova, 20, 11-21.
1127 https://doi.org/10.1111/j.1365-3121.2007.00781.x
1128 Latham, A.J., Riding, R., 1990. Fossil evidence for the location of the Precambrian-Cambrian
1129 boundary in Morocco. Nature, 344, 752–754.
1130 Laubier, M., Grove, T.L., Langmuir, C.H., 2014. Trace element mineral/melt partitioning for basaltic
1131 and basaltic andesitic melts: An experimental and laser ICP-MS study with application to the
1132 oxidation state of mantle source regions. Earth Planet. Sci. Lett., 392, 265-278.
1133 Leblanc, M., 1975, Ophiolites précambriennes et gîtes arseniés de cobalt (Bou Azzer, Maroc).
1134 Unpublished M.Sc. thesis, University of Montpellier, 329 p.
1135 Leblanc, M., 1976. Proterozoic oceanic crust at Bou Azzer. Nature, 261, 34-35.
1136 Leblanc, M., 1981. The Late Proterozoic ophiolites of Bou Azzer (Morocco): evidence for Pan-
1137 African plate tectonics. In: A. Kröner (Editor), Precambrian Plate Tectonics. Elsevier,
1138 Amsterdam, pp. 435-451.
1139 Leblanc, M., Billaud, P., 1982. Cobalt arsenide orebodies related to an upper Proterozoic ophiolite:
1140 Bou Azzer (Morocco). Econ. Geol., 77, 162-175.
1141 Leblanc, M., and Fischer, W., 1990. Gold and platinum group elements in cobalt arsenide ores:
1142 Hydrothermal concentration from a serpentinite source-rock. Mineralogy and Petrology, 42,
1143 197-209.
1144 Leblanc, M., Lbouabi, M., 1988. Native Silver Mineralisation along a Rodingite Tectonic Contact
1145 between Serpentinite and Quartz Diorite (Bou Azzer, Morocco). Econ. Geol., 83, 1379-1391.

1146 Levresse, G., 2001. Contribution à l'établissement d'un modèle génétique des gisements d'Imiter
1147 (Ag-Hg), Bou Madine (Pb-Zn-Cu-Ag-Au) et Bou Azzer (Co-Ni-As-Ag-Au) dans l'Anti-Atlas
1148 marocain. Unpublished M.Sc. thesis, CRPG-CNRS, Nancy, France, 191 p.
1149 Levresse, G. Bouabdellah, M., Gasquet, D., Cheilletz, A., 2017. Basinal brines at the origin of the
1150 Imiter Ag-Hg deposit (Anti-Atlas, Morocco): Evidence froim LA-ICP-MS data on fluid
1151 inclusions, Halogen signatures, and stable isotopes (H, C, O) – A discussion. Econ. Geol., 112,
1152 1269-1277.
1153 Maacha, L., Alansari, A., Saquaque, A., Soulaimani, A., 2012. The Bou Azzer Cobalt-Nickel-Arsenic
1154 District. In: Les principales mines du Maroc, Michard, A., Saddiqi, O., Chalouan, A., Rjimati,
1155 C., Mouttaqi, A. (Eds.). Nouveaux Guides Géologiques et Miniers du Maroc, pp. 91-97.
1156 Maacha, L., Elghorfi, M., Ennaciri , A., Sadiqqi, O., Soulaimani, A., Alansari, A., Bhilisse, M., 2015.
1157 Nouvelles données isotopiques et d'inclusions fluides des minéralisations cobaltifères de Bou
1158 Azzer. Apport à la géologie économique de la boutonnière. (Anti-Atlas central, Maroc). Notes
1159 et Memoires du service Géologique, 579, 133-139.
1160 Manatschal, G., 2004. New models for evolution of magma-poor rifted margins based on a review of
1161 data and concepts from West Iberia and the Alps. Intern. J. Earth Sci., 93, 432-466.
1162 https://doi.org/10.1007/s00531-004-0394-7
1163 Manatschal, G., Engström, A., Desmurs, L., Schaltegger, U., Cosca, M., Müntener, O., Bernoulli, D.,
1164 2006. What is the tectono-metamorphic evolution of continental break-up: The example of the
1165 Tasna Ocean–Continent Transition. J. Struct. Geol., 28, 1849-1869.
1166 Manheim, F.T., Lane-Bostwick, C.M., 1988. Cobalt in ferromanganese crusts as a monitor of
1167 hydrothermal discharge on the Pacific sea floor. Nature, 335, 59-62.
1168 Markl, G., Burisch, M., Neumann, U., 2016. Natural fracking and the genesis of five-element veins.
1169 Miner. Dep., 51, 703–712.
1170 Mifdal, A., Peucat, J.J., 1985. U-Pb and Rb-Sr dating of acidic volcanic rocks and Precambrian
1171 basement in Anti-Atlas of Morocco (Ouarzazate). Contribution for numerical dating of
1172 Precambrian-Cambrian boundary. Sciences Géologiques, Bulletins et Mémoires, 38, 185-200.
1173 Missenard, Y., Zeyen, H., Frizon de Lamotte, D., Leturmy, P., Petit, C., Sébrier, M., Saddiqi, O.,
1174 2006. Crustal versus asthenospheric origin of relief of the Atlas Mountains of Morocco. J.
1175 Geophys. Res.- Solid Earth, 111, B03401.
1176 Naldrett, A.J., 2005. A history of our understanding of magmatic Ni-Cu sulfide deposits. Can.
1177 Mineral., 43, 2069-2098.
1178 Oberthür, T., Melcher, F., Henjes-Kunst, F., Gerdes, A., Stein, H., Zimmerman, A., El Ghorfi, M.,
1179 2009. Hercynian age of the Cobalt-Nickel-Arsenide-(Gold) ores, Bou Azzer, Anti-Atlas,
1180 Morocco, Re-Os, Sm-Nd, and U-Pb age determinations. Econ. Geol., 104, 1065-1079.
1181 Pirrie, D., Butcher, A.R., Power, M.R., Gottlieb, P., Miller, G.L., 2004. Rapid quantitative mineral
1182 and phase analysis using automated scanning electron microscopy (QEMSCAN); potential

applications in forensic geoscience. Geological Society, London, Special Publication, 232, 123-136.

Pouit, G., 1966. Paléogéographie et répartition des minéralisations stratiformes de cuivre dans l'anti-Atlas occidental (Maroc). Chron Rech Min, 356, 279-289.

Relvas, J., 2000. Geology and metallogenesis at the Neves Corvo deposit. Unpublished M.Sc. Thesis, Universidade de Lisboa, Portugal. 319 p.

Richardson, C.J., Cann, J.R., Richards, H.G., Cowan, J.G., 1987. Metal-depleted root zones of the Troodos ore-forming hydrothermal systems, Cyprus. Earth Planet. Sci. Let., 84, 243-253.

Samson, S. D., Inglis, J. D., D'Lemos, R. S., Admou, H., Blichert-Toft, J., Hefferan, K., 2004. Geochronological, geochemical, and Nd-Hf isotopic constraints on the origin of Neoproterozoic plagiogranites in the Tasriwine ophiolite, Anti-Atlas orogen, Morocco. Precam. Res., 135, 133-147.

Saquaque, A., Admou, H., Karson, J., Hefferan, K., Reuber, I., 1989. Precambrian accretionary tectonics in the Bou Azzer-El Graara region, Anti-Atlas, Morocco. Geology, 17, 1107-1110.

Smedley, P.L., Kinniburgh, D.G., 2002. A review of the source, behaviour and distribution of arsenic. Natural waters, 17, 517-568.

Soulaimani, A., Michard, A., Ouanaimi, H., Baidder, L., Raddi, Y., Saddiqi, O., Rjimati, E.C., 2014. Late Ediacaran-Cambrian structures and their reactivation during the Variscan and Alpine cycles in the Anti-Atlas (Morocco). J. African Earth Sci., 98, 1-19. https://doi.org/10.1016/j.jafrearsci.2014.04.025

Thiéblemont, D., Chêne, F., Liégeois, J.P., Ouabadi, A., Le Gall, B., Maury, R.C., Jalludin, M., Ouattara Gbélé, C., Tchaméni, R., Fernandez-Alonso, M., 2016. Geological Map of Africa at 1:10 Million Scale, 35th International Geology Congress ed; CCGM-BRGM: Orléans, France.

Thomas, R.J., Fekkak, A., Ennih, N., Errami, E., Loughlin, S.C., Gresse, P.G., Chevallier, L.P., Liégeois, J.P., 2004. A new lithostratigraphic framework for the Anti-Atlas Orogen, Morocco. J. African Earth Sci., 39, 217-226.

Tourneur, E., 2019. Circulation de fluides aux abords de failles d'échelle crustale : contraintes structurales, microtectoniques, inclusions fluides et géochimiques sur les processus de formation du gisement de Bou Azzer (Ni-Co), Anti-Atlas, Maroc. Sciences de la Terre. Université Montpellier, 377 p.

Tourneur, E., Chauvet, A., Kouzmanov, K., Tuduri, J. Sizaret, S., 2019. Textural and mineralogical constraints on the mode of formation of the Bou Azzer Co-Ni arsenide mineralization (Anti-Atlas, Morocco): Tectonic implications. Proceeding of the 15th SGA biennial Meeting, 1, 17-20.

Triantafyllou, A., Berger, J., Baele, J., Diot, H., Ennih, N., Plissart, G., Monnier, C., Watlet, A., Bruguier, O., Spagna, P., Vandycke, S., 2016. The Tachakoucht - Iriri - Tourtit arc complex (Moroccan Anti-Atlas): Neoproterozoic records of polyphased subduction-accretion dynamics during the Pan-African orogeny. J. Geod., 96, 81-103.

1220 Triantafyllou, A., Berger, J., Baele, J.M., Bruguier, O., Diot, H., Ennih, N., Monnier, C., Plissart, G.,
1221 Vandycke, S., Watlet, A., 2018. Intra-oceanic arc growth driven by magmatic and tectonic
1222 processes recorded in the Neoproterozoic Bougmane arc complex (Anti-Atlas, Morocco).
1223 Precam. Res., 304, 39-63. https://doi.org/10.1016/j.precamres.2017.10.022
1224 Tucker, M.E., 1986. Carbon isotope excursions on Precambrian/Cambrian boundary beds, Morocco.
1225 Nature, 319, 48-50.
1226 Tuduri, J., 2005. Processus de formation et relations spatio-temporelles des minéralisations à or et
1227 argent en contexte volcanique Précambrien (Jbel Saghro, Anti-Atlas, Maroc). Unpublished
1228 M.Sc. thesis, CNRS, Orleans, France, University of Orleans, 468 p.
1229 Tuduri, J., Chauvet, A., Barbanson, L., Bourdier, J.L., Labriki, M., Ennaciri, A., Badra, L., Dubois,
1230 M., Ennaciri-Leloix, C., Sizaret, S., Maacha, L., 2018a. The Jbel Saghro Au(–Ag, Cu) and Ag–
1231 Hg Metallogenetic Province: Product of a Long-Lived Ediacaran Tectono-Magmatic Evolution
1232 in the Moroccan Anti-Atlas. Minerals, 8, 592.
1233 Tuduri, J., Chauvet, A., Barbanson, L., Labriki, M., Dubois, M., Trapy, P.H., Lahfid, A., Poujol, M.,
1234 Melleton, J., Badra, L., Ennaciri, A., Maacha, L., 2018b. Structural control, magmatic-
1235 hydrothermal evolution and formation of hornfels-hosted, intrusion-related gold deposits:
1236 Insight from the Thaghassa deposit in Eastern Anti-Atlas, Morocco. Ore Geol. Rev., 97, 171-
1237 198.
1238 Wafik, A., Admou, H., Saquaque, A., El Boukhari, A., Juteau, T., 2001. Cu-Fe sulfureous
1239 mineralisations and the associated alterations in the Bou Azzer and Khzama Proterozoic
1240 ophiolites, Anti-Atlas, Morocco. Ofioliti, 26, 47-62.
1241 Walsh, G.J., Benziane, F., Aleinikoff, J.N., Harrison, R.W., Yazidi, A., Burton, W.C., Quick, J.E.,
1242 Saadane, A., 2012. Neoproterozoic tectonic evolution of the Jebel Saghro and Bou Azzer-El
1243 Graara inliers, eastern and central Anti-Atlas, Morocco. Precam. Res., 216, 23-62.
1244
1245 **Figures Captions**
1246
1247 Figure 1: Localisation of the studied area at (A) the West African Craton scale (after Thiéblemont et
1248 al., 2016) and (B) at the Moroccan Anti-Atlas scale (after Hollard et al., 1985; Tuduri et al.,
1249 2018a). Different inliers are: AM: Agadir-Melloul; BD: Bas Drâa; If: Ifni; Ig: Iguerda; Im:
1250 Igherm; K: Kerdous; TA: Tagragra of Akka; TT: Tagragra de Tata; Z: Zenaga. C) Geological
1251 map of the Bou Azzer district modified after Leblanc (1975) and Admou et al. (2013).
1252
1253 Figure 2: Simplified block diagram showing the distribution of the main geological units of the Co-
1254 Ni-As (-Au-Ag) Bou Azzer district and also the main ore deposits studied in this study. All the
1255 underground occurrences here studied were indicated with depth level. See text for explanation.
1256

Figure 3: Photographs of host rocks. A) Faulted contact with normal motion between serpentinite and carbonated complex shell (*Ambed* location, see Fig. 2). B) Intrusive contact of quartz diorite in mafic rocks (*Taghouni* location). C) Massive serpentinite with layers of magnetite, talc- and carbonate-alteration and stereonet diagram of the serpentinite cleavage pole (Schmidt stereonet, lower hemisphere, *Taghouni* location). D) Contact with rodingite between serpentinite and quartz diorite (*Taghouni,* level 80). E) Linear contact between serpentinite and quartz diorite showing the development of alteration halo in both rocks (*BAE P3* location).

Figure 4: Photographs of surface structures. A) *Bou Azzer East* field zone showing the contact between serpentinite, siliceous complex shell, mafic rock and quartz diorite. The siliceous gangue is affected by carbonate-rich large-scale pocket (white line) and contains serpentinite fragments (green line). B) Large-scale pull-apart structure composed of a siliceous gangue and exhibiting massive and/or laminated texture (zoom in the red square). C) *Filon 7* aspect at surface after it junction with the *Filon 5*. D) Large view of the *Bou Azzer Centre* mine showing the *Filon 7* extension reaching several hundred metres long. E) *Quarry 52* image representing veins cutting the massive mineralisation and serpentinite.

Figure 5: Macroscopic aspect of the massive mineralisation and veins in underground galleries. A) Typical Co-Ni-Fe bearing massive mineralisation separating serpentinite and carbonated gangue (*Aghbar,* level 410). B) Similar massive mineralisation against siliceous gangue (*Bou Azzer East P6*, level 510). C) Veins showing brecciated texture (with diorite fragments mainly) and composed of Co-Fe bearing minerals and late euhedral calcite pocket (Cal) (*Bou Azzer East P3*, level 80). D) Mineralised pockets composed of quartz/chlorite/skutterudite border, followed by comb-quartz and Co-Fe arsenides. Late rhombohedral calcite with fragments of Co-Fe arsenide is visible in the centre of the pockets (*Filon 53*, level 240).

Figure 6: A) 3D sketch of mineralised contact on surface and in gallery for comparison. B) Stereonet poles contour diagram of the massive mineralisation and the veins measured orientation on the field and galleries (Schmidt stereonet, lower hemisphere).

Figure 7: Photographs of vein structures in mining galleries. A and B are photographs of the vertical plane. C and D are photographs and corresponding sketch (D) of horizontal plane (view realised towards the top of the mining gallery). A) Normal vein structure illustrated by the offset of the epidote-rich vein (Ep-Vein) (*Filon 53*, level 240). B) Similar motion showing by pull-apart structure (Same area, *Filon 53*, level 240). C) Mineralised vein trending east and showing dextral motion (*Bouismas area*, level 390). D) Mineralised vein trending north-east and showing left-lateral motion with interpretative sketch (*Bou Azzer East, Puit 3*, level 510).

Figure 8: Schematic diagram explaining the conjugate character of the vein system at Bou Azzer. Conjugate veins in the horizontal planes A systematic normal motions is observed in the vertical plane whereas NS and N070°E veins are dextral and sinistral, respectively, allowing to define a transtensional tectonic regime with a roughly NNE/SSW shortening direction.

Figure 9: Paragenetic sequence, texture and relative proportions of major elements (metals and sulphur) in the different structures of the Bou Azzer Co-Ni-As(-Au-Ag) district. Grey colour represents minerals of surrounding rocks, purple: Ni-stage, green; Co-stage, black: gangue minerals, blue: sulphide stage, orange: sodic-calcic alteration and pink: supergene alteration. (Ab: Albite, Adu: Adularia, As: Arsenic, Apy: Arsenopyrite, Bn: Bornite, Cal: Calcite, Cct: Chalcocite, Chl: Chlorite, Co: cobalt, Cob: Cobaltite, Ccp: Chalcopyrite, Dg: Digenite, Dol: Dolomite, Ep: Epidote, Ert: Erythrine, Fe: iron, Gd: Gersdorffite, Gn: Galena, K: potassium, Lo: Loellingite, Ni: nickel, Nk: Nickeline, Qz: Quartz, Ram: Rammelsbergite, S: Sulphide, Saf: Safflorite, Sku: Skutterudite, Sp: Sphalerite, Ttn: Titanite, Tlc: Talc, Tnt-Ttr: Tennantite - Tetrahedrite)

Figure 10: Mineral assemblages of the Ni-Co arsenide mineralisation at Bou Azzer. A) Quartz diorite composed of albite (Ab), quartz (Qz) and loellingite (Lo1) cross-cut by potassic feldspar (k-Fsp) (optical cathodoluminescence image, CL); B) Aspect of the serpentinite near massive mineralisation showing spinel (Spl) grain which is sometimes entirely replaced/transformed by rammelsbergite (see rectangle and zoom in Fig. 10C). Within the massive body, skutterudite is also fractured and fill by serpentinite (polarised light, PL); C) Isolated nuclei of rammelsbergite inside the serpentinite showing fracture filled by neoformed elongated serpentine (RL image). D) Laminated Massive Mineralisation (LMM) showing Ni-Co rich arsenide bands (nickeline, rammelsbergite, skutterudite, cobaltite) alternating with bands of calcite large crystal (Cal1) and sphalerite (RL). E) Disseminated spinel with magnetite-rich margin surrounded by rammelsbergite (Ram) and nickeline (Nk1) grains. F) Feathery rammelsbergite fragment (Ram) encapsulated inside successive crystallisation of skutterudite (Sku1), calcite (Cal1), infilling chalcopyrite (Ccp) and prismatic to cloudy loellingite (Lo1) ending by a massive gangue of euhedral banded skutterudite (Sku2) and calcite (Cal2) (RL image). G) RL image illustrating the brecciated character of the massive mineralisation (BMM) with rammelsbergite fragments surviving in core of a cobaltite (Cob1) - skutterudite (Sku2) - calcite (Cal1) - chalcopyrite (Ccp) matrix. Late calcite (Cal2) fills the interstitial open-space. H) Growing of star-shaped safflorite (Saf1) on rammelsbergite (not visible on the photography), followed by loellingite (Lo2) and large carbonate grain of the carbonated gangue (Cal2) (RL image, polarised).

Figure 11: Automated mineralogy: A) QEMSCAN mineral map of serpentinite in contact with the massive mineralisation at *Aghbar*. A strong talc alteration is observed in the left part of the sample (serpentinite) whereas a calcite impregnation is dominant in its right part (carbonated gangue of the mineralisation). Small (<2000 µm) spinel grains are preserved in the serpentinite whereas while they are replaced by large bornite grains, associated with skutterudite in the carbonate gangue. Cobaltite is disseminated in both part of the sample. B) QEMSCAN mineral map of the massive mineralisation at *Filon 53* composed mainly of very elongated rammelsbergite noddles surrounded by large skutterudite. Noddle distribution suggests that they were formed by replacement/transformation of initial fragments, possibly spinel grains (see text for explanation). Note that earlier carbonate can develop in contact with rammelsbergite and the final appearance of Cu-rich sulphides (i.e., chalcopyrite). C) QEMSCAN mineral map, Co and Ni element distribution maps for massive mineralisation at *Bouismass*. Skutterudite and rammelsbergite form zoned aggregates with successive Ni-rich and Co-rich growth zones. See text for explanation. Note that rammelsbergite forms isolated nucleus systematically surrounded by cobaltite and skutterudite. D) Transmitted-light image and QEMSCAN mineral map of vein structure at *Aghbar* showing textural relationship between skutterudite, spinel (chromite) and chlorite within a siliceous gangue. The Co map shows that skutterudite has Co-rich border. Note the late dolomite infill (sky blue colour on the QEMSCAN map). E) Transmitted-light image, QEMSCAN mineral map, Co and Ni element distribution maps from *Filon 7/5* vein structure. Small skutterudites (black arrow) are associated with the early dolomite grains and show not detectable Ni content. Inversely, cobaltite related to comb-quartz has significant Ni proportion. F) QEMSCAN mineral map and Co and Fe element distribution maps of a border of a vein structure (*Bouismass*), focused on skutterudite-loellingite relationship. Skutterudite is elongated, fractured and Co/Ni growth bands are less marked than in skutterudite from the massive mineralisation. Loellingite appearance is indicator of a Co/Fe transition.

Figure 12: Chemical composition of mineralisation from the serpentinite, the massive mineralisation, the vein system, the pockets and complex shells of the Bou Azzer area. A) As versus S (apfu) within different skutterudites. B) Fe+Ni versus Co (apfu) composition within skutterudite of the different type of deposits. C) Mg-Fe-Mn distribution within calcites (apfu). Data provide from EPMA analysis in Tourneur (2019).

Figure 13: Thin section illustrations of the carbonated mineralised gangue of the massive system and vein. A) Cobaltite (Cob2) and nickeline (Nk2) formed along fractures inside rammelsbergite minerals (RL image). Note the occurrence of late calcite (Cal4). B) Optical-CL image of a spinel (Spl) grain partially replaced by the carbonated gangue from the massive mineralisation.

A magnetite-rich margin (Mag) was identified and confirmed by EPMA. C) Laminated nickeline (Nk1) surrounded by skutterudite (Sku2) synchronous with calcite (Cal1) as demonstrated by successive and alternating growth bands (massive mineralisation, RL image). D) Skutterudite associated with dolomite (Dol1) and comb quartz in veins. Cobaltite (Cob2) is supposed to form during a second stage between comb quartz (Qz2) and by replacement of skutterudite (Sku3); E) Adularia (Adu) with a triangular shape forming along vein margin. Minerals inside the vein are quartz (Qz3) and calcite (Cal3) whereas adularia growth on albite mineral of the surrounding rock (Ab) (PL image). F) Rim of a geodic pocket texture exhibiting loellingite (Lo2) and cobaltite (Cob3) (Co-Fe arsenide in the picture) large minerals followed by comb quartz (Qz3) and large calcite (Cal3-4) crystallisation (RL image, polarised). G) Cold-CL image of carbonated gangue showing the brecciated aspect with earlier calcite fragment (Cal2) and the late crystallisation of euhedral large calcite grains (Cal2). H) Serpentinite fragments in the carbonated gangue (Cal2) (PL image).

Figure 14: Additional textural observations. A) High magnification view of the red rectangle area indicated of the Figure 11B. Note that detailed texture of rammelsbergite grains show the existence of two generations: a first mineral formed the elongated grains and some second acicular crystals with higher Co values overgrown on them. This texture indicates rapid crystallisation under oversaturated conditions. B) Cold-CL image of calcite gangue of massive mineralisation showing the occurrence of previous ghost mesh textures now entirely transformed in calcite minerals (see the interpretative sketch). C) BSE image of serpentinite where the texture could be transformed by carbonation in order to form the ghost mesh texture of the Figure 14B.

Figure 15: Interpretative three-stage petro-structural model of the Bou Azzer Co-Ni mineralisation formation. All indications in red within this figure are interpretations whereas the ones in black are observations. A and A1) Pre-mineralisation stage showing the significant role of the existence of elongated lenses of serpentinite breccia at the contact between serpentinite and quartz diorite. Note the presence of spinel minerals, magnetite layers (future Ni-rich minerals) and open space (future mineralised pockets). B) In situ formation of the massive mineralisation by percolation, leaching, replacement, transformation of the brecciated lenses (see text for details). Two stages were identified, a Ni-Co-As one with formation of nickeline and rammelsbergite (B1) and a Co-As-Fe-S stage with crystallisation of skutterudite and cobaltite forming massive bodies and associated to the formation of carbonated and/or siliceous gangue (B2). Fragments of serpentinite were still visible in the gangue. C and C1) Vein formation stage under the control of NNNE-SSW transtensional tectonic event. Co-rich minerals formed followed by the general emplacement of late Fe-S minerals (sulphide stage).

Figure 16: Hypothetic tectonic context favourable for the formation of the mineralisation system of the Bou Azzer district (Morocco). Normal fault was supposed to develop zone of tectonic breccia and mylonitic deformational zones that will serve as trap for the future massive mineralisation. In such a scenario, fault motion is considered as normal (see text for explanation) and Brecciated Massive Mineralisation (BMM) were formed in brecciated lenses whereas Laminated Massive Mineralisation (LMM) developed in previously-formed mylonitic zone. Note the frequent occurrence of mafic rocks at the limit between the serpentinite and the intrusive quartz diorite.

Table 1: Information on the different locations analysed in this study: sampling depths, coordinates of wells in WGS84, mineralisation type are indicated.

Highlights

- Two types of mineralisation characterised the Bou Azzer District
- Massive mineralisations are forming by remobilisation processes from relics of spinels
- Veins system are linked with a mode of formation associated with tectonics
- Continuous evolution from Ni-rich to Co-rich mineralisations in all structures
- The mineralised bodies correspond to ancient sedimentary breccia
- The mineralised bodies are formed in slope of detachement faults that allow to exhume mantle rocks

Declaration of interests

☒ The authors declare that they have no known competing financial interests or personal relationships that could have appeared to influence the work reported in this paper.

☐The authors declare the following financial interests/personal relationships which may be considered as potential competing interests:

1436

LOCALITY	WELL		DEPTH (m)	LONGITUDE	LATITUDE	EINS	MASS. MIN.
Taghouni	-		-80/-120	30°31'35"N	6°55'48"W		
Bou Azzer Centre	P 3		-420	30°31'13"N	6°54'48"W		✓
Bou Azzer East	P 3	302	-320/-	30°30'59"N	6°53'44"W		✓
Bou Azzer East	P 6		-510	30°3	6°5		✓

1437

1438

			0'57"N	3'35"W	
Aghbar	P 100	-325/-365/-405	30°31'35"N	6°49'06"W	✓
Oumlil	-	-77	30°31'22,55"N	6°47'6,89"W	
Bouismass	P 2	-390	30°30'55"N	6°47'18"W	✓
Bouismass	P 1	-80	30°30'59"N	6°45'15"W	✓
Tamdrost	-	-20	30°31'23.9"N	6°47'06.8"W	
Aït Ahmane					
Filon 53	-	-115/-200/-240	30°28'01"N	6°35'16"W	✓
Zone D	-	-200	30°29'50"N	6°37'21"W	
Quarries					
Bou Azzer Est	-	surface	30°31'01.8"N	6°53'41.2"W	
Filon 52	-	surface	30°28'15"N	6°35'41"W	✓
Filon 55	-	surface	30°31'22"N	6°47'13"W	✓
Surface					
Filon 2	-	surface	30°31'24.4"N	6°54'32.5"W	✓
Filon7 and *Filon 5* (*Bou Azzer Centre)*	-	surface	30°31'13"N	6°54'48"W	
Ambed	-	surface			
Trench					
Bou Azzer Est trench	-	surface	30°31'15.7"N	6°53'46.8"W	

Appendix

Appendix 1.1: Structural data on the direction to the north, the dip angle and the dip angle orientation of the massive mineralisation

Massive mineralisation	Direction	Dip angle	Dip angle orientation
BAE P6 (-510m)	N60	60	SE
BAE P6 (-510m)	N100	70	SE
Filon 53 (-145m)	N90	60	N
Aghbar (-365m)	N10	60	W

Bouismass (-390m)	N100	30	S
Aghbar (-325m)	N40	60	NW
Filon 53 (-240m)	N70	75	SE
BAE P3 (-320m)	N105	50	SSW

1446

1447 Appendix 1.2: Structural data on the direction to the north, the dip angle and the dip angle
1448 orientation of the veins system

Vein system	Direction	Dip angle	Dip angle orientation
BAC P3 (-420m)	N00	40	W
BAC P3 (-420m)	N10	60	W
BAE P6 (-510m)	N10	70	E
BAE P6 (-510m)	N10	70	W
BAE P6 (-510m)	N10	70	W
BAE P6 (-510m)	N10	85	E
BAE P6 (-510m)	N10	85	E
BAE P6 (-510m)	N100	30	S
BAE P6 (-510m)	N105	50	SSW
Taghouni (-80m)	N120	60	NE
Taghouni (-80m)	N120	75	NE
Taghouni (-80m)	N130	70	SW
Taghouni (-80m)	N135	40	SW
Taghouni (-80m)	N160	34	WSW
Aghbar (-365m)	N160	60	W
Bouismass (-390m)	N160	60	WSW
Bouismass (-390m)	N160	80	WSW
Bouismass (-80m)	N170	80	W
Bouismass (-80m)	N170	90	
Bouismass (-	N1	90	W

80m)	70			
Bouismass (-80m)	N174	70	ENE	
Bouismass (-80m)	N175	85	E	
Taghouni (-80m)	N20	60	W	
Filon 7 - surface	N20	80	W	
BAE P3 (-302m)	N22	88	W	
BAE P3 (-302m)	N30	60	NW	
BAE P3 (-302m)	N30	60	SE	
BAE P3 (-302m)	N35	80	NW	
Oumlil (-77m)	N40	50	NW	
Tamdrost (-20m)	N40	60	NW	
Zone D (-200m)	N40	60	NW	
Zone D (-200m)	N40	60	NW	
BA centre P3	N40	60	NW	
BA centre P3	N40	65	SE	
Filon 53 (-200m)	N40	70	SE	
Filon 53 (-115m)	N40	80	NW	
Filon 55 - surface	N40	80	NW	
Filon 52 - surface	N45	85	NW	
BAE P3 (-302m)	N50	80	NW	

1449

1450

1451 Appendix 2: signal in Raman spectrometry and associated peaks of lizardite/chrysotile

1452 serpentinite

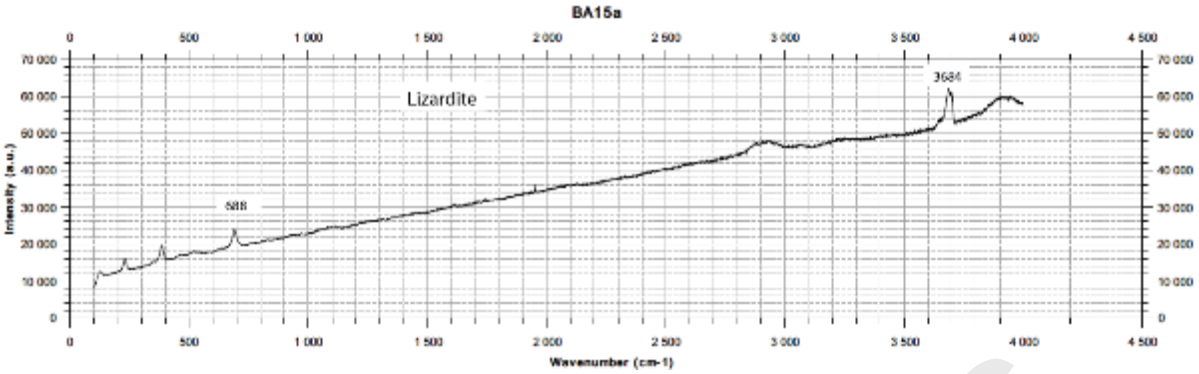

1453

1454 Appendix 3: As concentration of common rocks and minerals and from Bou Azzer

Rocks and minerals	As concentration (ppm)	Source
Oxide minerals		
Fe oxide (undifferentiated)	up to 2000	Boyle and Jonasson (1973)
Magnetite	2.7 - 41	Baur and Onishi (1969)
fibrous magnetite	400	Leblanc (1975)
magneite veins	20	Gahlan et al. (2006)
Silicate minerals		
Quartz	0.4-1.3	Baur and Onishi (1969)
Feldspar	<0.1-2.1	Baur and Onishi (1969)
Biotite	1.4	Baur and Onishi (1969)
Amphibole	1.1-2.3	Baur and Onishi (1969)
Olivine	0.08-0.17	Baur and Onishi (1969)
Pyroxène	0.05-0.8	Baur and Onishi (1969)
sulphide in serpentinite	50 and 1000	Leblanc &Fischer (1990)
Carbonate minerals		
Calcite	1 to 8	Boyle and Jonasson (1973)
Dolomite	<3	Boyle and Jonasson (1973)
Igneous rocks		
Apatite	<1 - 1000	Baur and Onishi (1969)
ultrabasic (peridotite, dunite, kimberlite, etc…)	0.03-15.8	smedley et al. (2002)
Serpentinized ultramafic rocks	10 - 450	Hattori et al. (2005); Sullivan (2007)
basalt	0.18-113	smedley et al. (2002)
gabbros	0.06-28	Onishi and Sandell (1955)
diorite, granodiorite	0.09-13.4	Boyle and Jonasson (1973)
rhyolite	3.2-5.4	Ure and Berrow (1982)
Neoproterozoic granitoid intrusions	<10 to ~25	Beraaouz et al. (2004)
Sedimentary rocks		
sandstone	0.6-120	Onishi and Sandell (1955)
Volcanic rocks		
ouarzazate group	100 - 300	Leblanc & Billaud (1982)

1455

1456

1457